Review

Recent Advances in Super Broad Infrared Luminescence Bismuth-Doped Crystals

Puxian Xiong,[1,2] Yuanyuan Li,[1,2] and Mingying Peng[1,*]

SUMMARY

Bismuth (Bi)-doped materials are capable of exhibiting broadband near-infrared (NIR) luminescence in 1,000–1,700 nm; driven by the potential use in lasers and broadband optical amplifiers for modern fiber communication systems, Bi-activated NIR luminescencent glasses and related devices have attracted much attention. Compared with glass systems, Bi-doped crystals as gain media usually have more regular crystal structures to produce stronger NIR signals, and developing such materials is highly desirable. Regarding the recent advances in Bi-doped NIR crystals, here, for the first time, we summarized such crystals listed as two main categories of halogen and oxide compounds. Then, by comparing the substitution site, coordination environment, emission and excitation luminescence peaks, emitting center species, and decay times of these known Bibased NIR crystals, discussion on how to design Bi-doped NIR crystals is included. Finally, the key challenges and perspectives of Bi-doped NIR crystals are also presented. It is hoped that this review could offer inspiration for the further development of Bi-doped NIR luminescent crystals and exploit its potential applications.

INTRODUCTION

The rapid development of the information age requires increasingly large-capacity optical fiber communication systems. The following two points need to be considered in this optical fiber communication system: (1) the gain bandwidth of the optical fiber amplifier should be as wide as possible to cover a broader near-infrared (NIR) communication window and (2) the corresponding NIR luminescence signal can be used as the laser light source. Making better use of the low-loss area of the optical fiber solves the problem of insufficient bandwidth in the current large-capacity optical fiber communication signal transmission process (Cao et al., 2018b; Fermann and Hartl, 2013; Peng et al., 2004; Udem et al., 2002). Fiber lasers were mainly based on rare-earth-doped fibers until 2005. However, the spectral region of 1,150–1,500 nm, which is promising for applications in communication and medicine, is hard to be covered for rare-earth-doped fiber lasers. Besides, lots of other NIR luminescent materials, with or without metal doping, have been adopted. Afterward, Bi-doped glasses were discovered to emit in the region of 1,000–1,700 nm, covering the optical communication O, E, S, C, L bands. Moreover, Bi-doped crystals own the advantage of tunable broadband emission due to their various valence states (Cao et al., 2019; Fujimoto and Nakatsuka, 2001; Murata et al., 1999; Peng et al., 2004; Wang et al., 2018b; Xiong et al., 2020; Zheng et al., 2020; Zhou et al., 2020). Therefore, Bi-doped glasses with broad NIR photoluminescence (PL) have been identified as potential optical amplifier gain media during the past decades (Cao et al., 2018a, 2018b; Peng et al., 2005; Peng and Wondraczek, 2009). In 1999, Murata et al. found a Bi-doped silica glass emitting ~1,132 nm with a life time of 650 μs (Murata et al., 1999). Due to the theoretical calculations, generation of optical pulses with a short 13 fs duration is possible. Also, Fujimoto et al. experimentally confirmed this by showing optical amplification at 1,300 nm under excitation of 800-nm laser diode pumping (Fujimoto and Nakatsuka, 2003). Fiber laser has excellent beam quality, and it owns the highest efficiency among solid-state lasers. The first fiber laser was achieved by E. Snitzer et al. in 1961 using Nd-doped glass optical fiber as active medium (Snitzer, 1961). The development of low-loss glass optical fibers and optical fiber communication promoted the appearance of high-efficiency fiber laser. In 2005, Dvoyrin et al. first achieved NIR Bi-doped silica-based fibers, which exhibit broadband emission of 200 nm full width at half maximum (FWHM) with the maximum in the region of 1.1–1.2 μm (Dvoyrin et al., 2005). Then, Dianov et al. realized continuous wave lasing in the spectra (1,150–1,300 nm) (Dianov et al., 2005). Furthermore, Peng et al. first enriched the Bi-doped glasses to multi-component germanate glasses with an FWHM of 300 nm (Peng et al., 2005). These discoveries have attracted the attention of worldwide researchers in

this field. Thus, Bi-doped fibers have been extended to non-silicate components, which get an advantage of lower melting temperature, less Bi volatilization, and easier fiber drawing. Subsequently, international research teams including domestic professors such as Qiu (Meng et al., 2005), Xia (Xia and Wang, 2006), and Peng (Peng et al., 2011) have carried out a lot of research work on related Bi-doped NIR glass systems. Notably, regarding the NIR origin, Peng et al. discussed it in bismuthate glass and Bi-doped glass in 2009 (Peng et al., 2009). Glass samples with compositions (in wt %) of $54Bi_2O_3 \cdot 24B_2O_3 \cdot 5SiO_2 \cdot 17PbO$ (BG1) and $52Bi_2O_3 \cdot 23B_2O_3 \cdot 4SiO_2 \cdot 17PbO \cdot 4Sb_2O_3$ (BG2) were synthesized. By comparing the absorption spectra of these Bi-doped glasses with spectral data of Bi^+ and Bi^0 (atomic Bi), they found that Bi^0 was more preferable to be the NIR origin. Besides, the emission and fluorescence lifetimes also support Bi^0 as NIR emission center. To further confirm this, Sb_2O_3 is introduced into BG2 as oxidizing agents, which will be oxidized into Sb_2O_5 at ~1,100°C. Sb^{5+} subsequently oxidizes Bi^0 to Bi^{3+}, leading to the elimination of NIR emission. Taking into account the aforementioned results, they ascribed NIR emission center and broadband NIR emission to Bi^0 species and transition from $^2D_{3/2}(1)$ to $^4S_{3/2}$, respectively. Till now, some comprehensive reviews also can be referred to in this developing field. For example, in 2011, Peng reviewed the origin of NIR emission in Bi-doped materials. Possible NIR centers were divided into higher valence group (Bi^{5+} and $Bi^{5+}O_n^{2-}$) and lower valence group (Bi^+, BiO, bismuth ion dimers, and Bi^0). The author suggested that compared with higher-valence bismuth and BiO, other lower-valence bismuth (especially Bi^0) is more reasonable to be the NIR origin (Peng et al., 2011), followed by the preliminary review on Bi-doped NIR amorphous solids from Qiu et al. in 2014 (Sun et al., 2014). Krasnikov et al. also discussed the possible NIR centers of Bi-doped glasses in 2020 (Krasnikov et al., 2020). However, the NIR emission efficiency of Bi-doped glasses is reaching its limitation due to the increasingly higher demand for large-capacity optical fiber communication signal transmission.

For this, Bi-doped crystals featuring more regular crystal structure should be considered. As NIR emissions of Bi in crystals are usually higher than those in glasses, developing such Bi crystals is highly worthwhile, although no reviews focusing on Bi-doped NIR luminescent crystals have been reported till now (Cao et al., 2018c; Wang et al., 2018a; Zhou et al., 2018). In 2005, to our knowledge, the first Bi-doped NIR (1,100–1,500 nm, λ_{ex} = 808 nm laser) luminescent crystal was found by Peng et al. in SrB_4O_7. They also conducted the first study of NIR Bi-doped silicate transparent glass-ceramics containing spinel phase ($ZnAl_2O_4$) (Peng et al., 2007). From these studies, some basic rules of stabilizing the NIR Bi luminescence center are summarized: that is, the material to be doped must contain large-sized cation lattice sites. Subsequently, it was only in 2008 that Russian scientists Okhrimchuk et al. discovered the second Bi-doped NIR crystal ($RbPb_2Cl_5$) (Okhrimchuk et al., 2008). Since then, series of Bi-activated NIR crystals were reported, and they are listed in Table 1. Notably, Peng et al. first attributed the NIR luminescence center to Bi^0 in Bi-doped crystal ($Ba_2P_2O_7$) in 2010, and this was the first time that Bi^0 model was adopted in Bi-doped NIR crystals (Peng et al., 2010). Their further work published in 2012 (Zheng et al., 2012) and 2019 (Wang et al., 2019) also repeatedly demonstrated the credibility of Bi^0 as an NIR Bi center as they insisted on. In addition, Bi^+ ions stably existing on Ba^{2+} sites were confirmed to possess NIR emission during the conversion from Bi^{2+} to Bi^0 via Bi^+ (Zheng et al., 2016). However, reviewing all the developments in this field to the present, one could not escape the rule that large-sized cation sites must be contained in the hosts. In this review, to our knowledge, recent advances of all the known Bi-doped NIR luminescent crystals are discussed in detail based on two main categories of halogen and oxide compounds. The crystal structure information of host (crystal system, space group, and point symmetry) and the chemical environment of to-be-substituted lattice sites (coordination number and Shannon radii) were systematically analyzed. By comparing the NIR spectral characteristics of these NIR crystals, it is hoped that this review would provide at least some inspirations for researchers to focus on this field.

KNOWN BI-DOPED NIR LUMINESCENT CRYSTALS
Halogen Compounds
Fluorides

Fluoride crystals doped with Tl and Pb were found to demonstrate NIR emission since the 1980s (Fockelet et al., 1989; Gelleilmann and Luty, 1981). Bismuth has the same electron configuration with Tl and Pb. Thus Su et al. prepared Bi-doped BaF_2, which showed broadband NIR emission centered at 1,070 and 1,500 nm (λ_{ex} = 500, 700, and 808 nm) (Figure 1A) (Ruan et al., 2009). The undoped crystal did not show any NIR emission. No Pb was found in crystal according to the inductively coupled plasma atomic emission spectrometry, although PbF_2 was used as oxygen scavenger. Furthermore, NIR emission intensity was highly reduced after heat treatment in air, indicating the structural differences of Bi-related centers (Figure 1B). They

Category		Host	Crystal System, Space Group, (Point Symmetry)	Sites (CN, Radii)	Em/Ex (nm)	Emitter	Decay Time (µs)	Year	Ref.
I	Fluorides	BaF$_2$	Cubic $Pm\overline{3}m$	Ba^{2+} (8, 1.42)	1,070, 1,500/808	Bi^{2+}, Bi$^+$	2.5, 2.1	2009	(Ruan et al., 2009)
		PbF$_2$	–	Pb^{2+} —	1,090, 1,485/600	Bi$^+$	4.7, 6.5	2018	(Zhang et al., 2018a, 2018b)
		SrF$_2$	Cubic $Pm\overline{3}m$	Sr^{2+} (8,1.26)	1,050/700	Bi^{2+}, Bi$^+$	25	2016	(Firstov et al., 2016)
	Chloride	Ba$_5$(PO$_4$)$_3$Cl	Hexagonal $P63/m$ (C3)	Ba^{2+} (6,1.35)	1,250/690	Bi$^+$	–	2013	(Li et al., 2013)
		Ba$_{10}$(PO4)$_6$Cl$_2$	Hexagonal $P6_3/m$ (C3)	Ba^{2+} (6,1.35)	~1,250/690	Bi$^+$	–	2012	(Li et al., 2012)
		AgCl	Cubic $Fm\overline{3}m$	Ag$^+$ (6, 1.15)	800–1,200/390–400	Bi$^+$	10.3	2013	(Plotnichenko et al., 2013a)
		TlCl	Cubic $Pm\overline{3}m$	Tl$^+$ (8, 0.98)	1,180/400–800	Bi$^+$	200–350	2013	(Plotnichenko et al., 2013b; Vtyurina et al., 2016)
		CsCdCl$_3$	Hexagonal $P6_3/mmc$, (D_{3h}, C_{3v})	Cs$^+$ (12, 1.88)	800–1,200/615	Bi$^+$	~360	2014	(Romanov et al., 2014)
		RbY$_2$Cl$_7$	$Pnma$, (Cs)	Rb$^+$ —	990/660	Bi$^+$	469	2016	(Romanova et al., 2016)
		KAlCl$_4$	Monoclinic P_{21}, ($C1$, $C1^*$)	K$^+$ (7, 1.46)	980/~600	Bi$^+$	525	2013	(Veber et al., 2012; Vtyurina et al., 2016)
		KMgCl$_3$	Orthorhombic $Pnma$, (Cs)	K$^+$ (8, 1.51)	950/~600	Bi$^+$	400	2013	(Romanov et al., 2013)
		Ba$_2$B$_5$O$_9$Cl	Orthorhombic $Pnn2$	Ba^{2+} (9, 1.47)	1,030/665	Bi^0	30.19	2012	(Zheng et al., 2012)
		Ba$_2$B$_5$O$_9$Cl	Orthorhombic $Pnn2$	Ba^{2+} (9, 1.47)	600–1,200/330	Bi$^+$	>1000	2016	(Zheng et al., 2016)
		Sr$_2$B$_5$O$_9$Cl	Orthorhombic $Pnn2$	Sr^{2+} (9, 1.31)	1,000–1700/460	Bi$^+$, Bi^0	5.9–17.2	2019	(Wang et al., 2019)
		RbPb2Cl$_5$	Cubic $Pm\overline{3}m$	Pb^{2+} (6, 1.19)	1,080/808	Bi$^+$, Bi^{2+}	140	2008	(Okhrimchuk et al., 2008)
		KCl	Cubic $Fm\overline{3}m$	K$^+$ (6, 1.38)	1,100, 1,300/500	Bi^{2+}(1)	10–20	2016	(Firstov et al., 2016)
		RbAlCl$_4$	Orthorhombic $Pnma$, (Cs)	Rb$^+$ —	950/597,642	Bi$^+$	–	2016	(Vtyurina et al., 2016)
		CsAlCl$_4$	Orthorhombic $Pnma$, (Cs)	Cs$^+$ (8, 1.74)	945/598,642	Bi$^+$	–	2016	(Vtyurina et al., 2016)
		RbMgCl$_3$	Hexagonal $P6_3/mmc$, (D_{3h}, C_{3v}^*)	Rb$^+$ (12, 1.72)	905/610,646	Bi$^+$	–	2016	(Vtyurina et al., 2016)
		CsMgCl$_3$	Hexagonal $P6_3/mmc$, (D_{3h})	Cs$^+$ (12, 1.88)	920/605,653	Bi$^+$	–	2016	(Vtyurina et al., 2016)
		KCdCl$_3$	Orthorhombic $Pnma$, (Cs)	K$^+$ (8, 1.51)	950/615,687	Bi$^+$	–	2016	(Vtyurina et al., 2016)
		RbCdCl$_3$	Orthorhombic $Pnma$, (Cs)	Rb$^+$ (9, 1.63)	1,015/605,670	Bi$^+$	–	2016	(Vtyurina et al., 2016)
	Bromides	CsCdBr$_3$	Hexagonal $P6_3/mmc$, (D_{3h})	Cs^{2+} (12, 1.88)	~1,053/532–690	Bi$^+$	~250	2015	(Romanova et al., 2015b)
	Iodides	CsI	Cubic $Pm\overline{3}m$	Cs$^+$ (8, 1.74)	1,216, 1,560/808	CE	130, 220	2011	(Su et al., 2011)
		TlCdI$_3$	Orthorhombic $Pnma$	Tl$^+$ (8, 0.98)	~1,175/400–800	Bi^{2+}	~30	2017	(Romanov et al., 2017)
		CsPbI$_3$	Orthorhombic $Pnma$	–	1,185/510	PD	–	2016	(Zhou et al., 2016)

Table 1. Known Compounds of Bi-Doped Near-Infrared Luminescent Crystals

| Category		Host	Crystal System, Space Group, (Point Symmetry)	Sites (CN, Radii)	Em/Ex (nm)	Emitter	Decay Time (µs)	Year	Ref.
II	Borates	α-BaB$_2$O$_4$	Trigonal $R3c$	Ba^{2+} (8, 1.42)	1,139/808,980	Bi$^+$	526	2009	(Su et al., 2009a)
		SrB$_4$O$_7$	Orthorhombic $Pmn2_1$	Sr^{2+} (9, 1.31)	1,100–1,500/808	Bi$^{x<3+}$	>600	2005	(Su et al., 2009b)
	Silicates	KGaSi$_2$O$_6$	Monoclinic $C2/m$	K$^+$ (9, 1.55)	1,170/532	Bi$^+$	~400	2015	(Romanov et al., 2015a)
	Aluminates	Gd$_{0.1}$Y$_{0.9}$AlO$_3$	–	Y^{3+} —	1,005, 1,565/600	Bi$^+$	–	2018	(Chen et al., 2018; Zhang et al., 2018a, 2018b)
		XAl$_{12}$O$_{19}$	Hexagonal $P63/mmc$	Al^{3+} (6, 0.535)	770/332	Bi^{3+}	2.6–3.02	2020	(Wei et al., 2020)
	Aluminum silicates	KAlSi$_2$O$_6$	Cubic $Ia\bar{3}d$	K$^+$ —	1,066/635	Bi$^+$	~400	2015	(Romanov et al., 2015a)
		CsAlSi$_2$O$_6$	Cubic $Ia\bar{3}d$	Cs$^+$ (6, 1.67)	1,230/532	Bi$^+$	~400	2015	(Romanov et al., 2015a)
	Phosphates	Ba$_2$P$_2$O$_7$	Hexagonal $P\bar{6}2m$	Ba^{2+} (10, 1.52)	~1,100/723	Bi^0	634	2010	(Peng et al., 2010)
		BaBPO$_5$	–	P^{5+}, B^{3+}	1,164/478–710	[BiO$_x$]	81–116	2016	(Liu et al., 2016)
	Tungstates	PbWO$_4$	–	–	1,360, 1,570/940	Bi$^+$	–	2012	(Xiong et al., 2012)
	Germanates	Y$_4$GeO$_8$	–	Y^{3+}	1,155/808	Bi$^+$	–	2011	(Xu et al., 2011)
		CsGaGe$_2$O$_6$	Cubic $I\bar{4}3d$	Cs$^+$	~1,250/475–820	Bi$^+$	–	2019	(Romanov et al., 2019)

Table 1. Continued
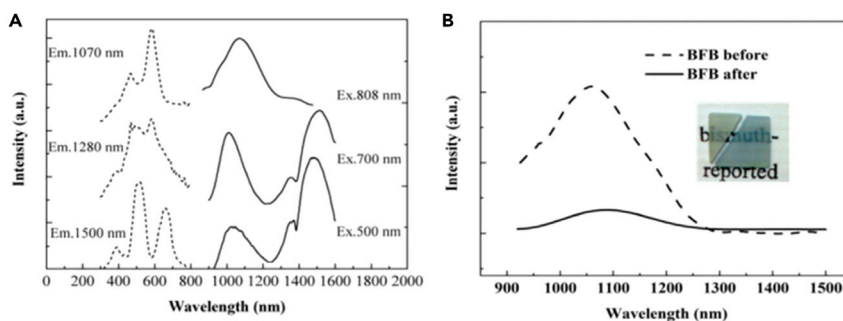
Figure 1. NIR Luminescent Properties of Bi:BaF$_2$

(A) NIR photoluminescence spectra of Bi:BaF$_2$ crystal excited at 500, 700, and 808 nm and measured excitation spectra of Bi:BaF$_2$ crystal monitored at 1,070, 1,280, and 1,500 nm.

(B) NIR emission spectra of Bi:BaF$_2$ samples before and after heat treatment. The insert shows the photographs of the samples. Reproduced with permission (Ruan et al., 2009). Copyright 2009, Optical Society of America.

suggested Bi^{2+} or Bi$^+$ centers adjacent to F vacancy defects as NIR origins. Also, the number of point defects will be highly reduced after heat treatment, leading to the decrease of NIR emission intensity.

Bi:SrF$_2$ crystal synthesized by Firstov et al. (2016) showed similar performance and active center as that in BaF$_2$:Bi. Two absorption bands peaked at 380 and 530 nm appeared after irradiation, whereas the 240 nm absorption band remained as before (Figure 2A). They indicated that the occurrence of the excitation bands at 380 and 530 nm are probably caused by the formation of perturbing vacancies adjacent to Bi^{2+} ion. Figure 2B demonstrates NIR emission centered at 1,050 nm from the irradiated Bi:SrF$_2$ crystal under 700 nm excitation. They suggested that new type of active centers (Bi$^+$ ion accompanied by two vacancies) could be formed by γ-irradiation.

In 2018, Zhang and co-workers synthesized Yb/Bi co-doped PbF$_2$ single crystal using Bridgman method (Zhang et al., 2018a, 2018b). Figure 3 shows the NIR emission spectra of prepared samples. It can be seen that Yb co-doping visibly increases NIR emission intensity. Yb^{3+} ions could act as sensitizer transferring energy to Bi-related active centers. At the same time, Yb^{3+} ions act as a charge-compensated ion for Bi ion, which is beneficial to the stabilization of Bi$^+$ valence state. With Yb^{3+} ions occupying Pb^{2+} sites and the formation of Yb$^+_{Pb}$, positive charge becomes excess. To maintain the electrical neutrality of the system, the valence conversion from Bi^{2+} to Bi$^+$ occurred. Bi$^+$ ions occupy Pb^{2+} sites leading to Bi$^-_{Pb}$ and realizing charge compensation. Both the energy transfer and valence conversion to lower state help enhance NIR emission intensity.

For above-mentioned synthesized crystals, it can be seen that heat treatment, irradiation, and codoping play a significant role in luminescence property by changing the number of point defects and converting
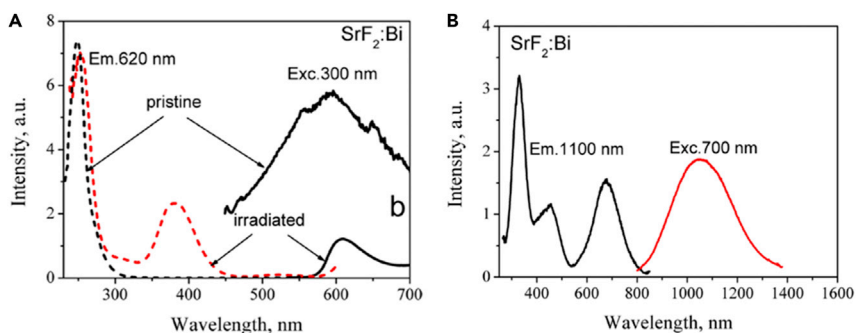

Figure 2. Luminescent Characteristics of Bi:SrF$_2$

(A) Typical emission (λ_{ex} = 300 nm) and excitation (λ_{em} = 620 nm) spectra of the pristine and irradiated Bi:SrF$_2$ crystal.

(B) PL emission (λ_{ex} = 700 nm) and excitation (λ_{em} = 1,100 nm) spectra of the irradiated Bi:SrF$_2$ crystal. Reproduced with permission (Firstov et al., 2016). Copyright 2016, IOP Science.
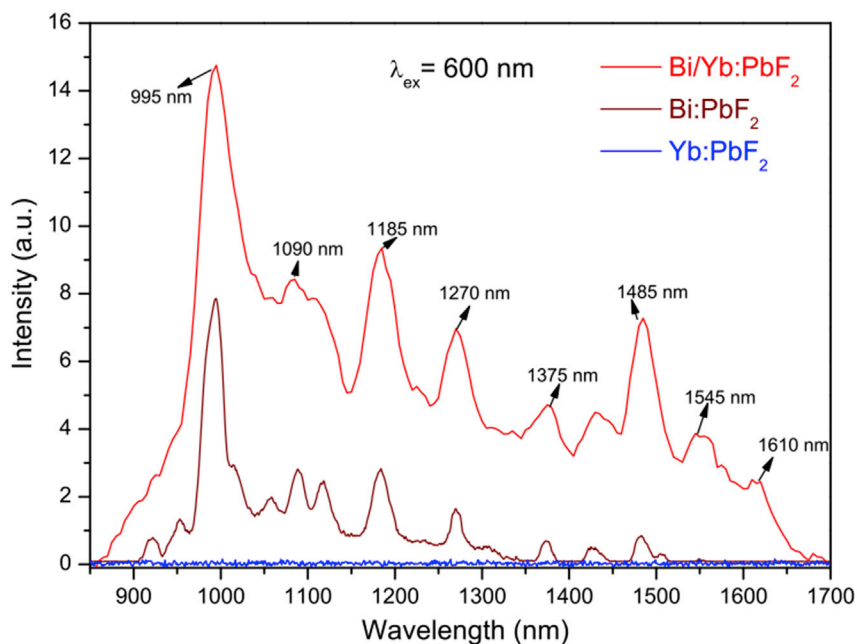
Figure 3. NIR Emission of Yb/Bi:PbF₂, Bi:PbF₂, and Yb:PbF₂ Crystals under 600 nm Excitation.
Reproduced with permission (Zhang et al., 2018a). Copyright 2018, Optical Society of America.

the valence of Bi ion. Heat treatment in air probably destroys Bi-related NIR active centers, whereas γ-irradiation may help produce NIR active centers, and both these aspects bring about chemical environment changes to the substituted sites.

Chlorides

To our knowledge, the first Bi-doped chloride of Bi:RbPb₂Cl₅ was found by Okhrimchuk et al. in 2008 (Okhrimchuk et al., 2008). Bi:RbPb₂Cl₅ is a single crystal grown by Bridgman technique. An intense NIR emission band centered at ~ 1,080 nm was observed under excitation at 808, 833, or 919 nm (Figure 4A), and four PL excitation peaks can be obtained in this system. The decay spectra follow an exponential character up to 2 magnitude orders with a lifetime of 140 μs. Based on the experimental data from absorption luminescence, PL excitation, and PL, together with the comparison of energies of multiplets between free Bi^+ and Pb^+ ions, they finally attributed the NIR PL to the $^3P_1 \rightarrow \, ^3P_0$ transition in Bi^+. Afterward, in 2012, Peng et al. proposed that Bi^0 could also act as the NIR center in chloride of Ba₂B₅O₉Cl (Zheng et al., 2012). Although they
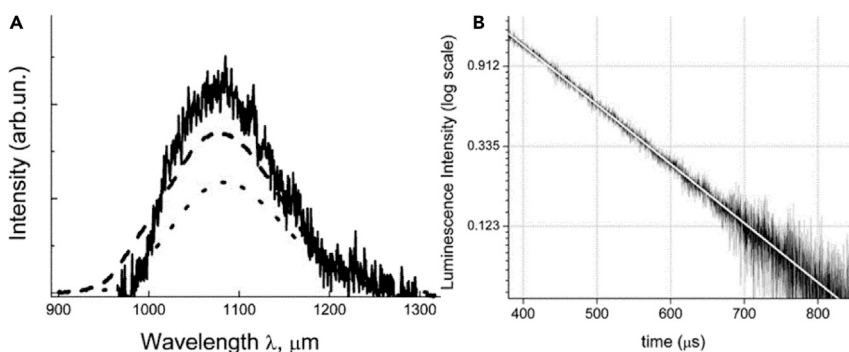

Figure 4. Luminescent Features of Bi:RbPb₂Cl₅
(A) Luminescence spectra of a Bi:RbPb₂Cl₅ crystal under excitation at 808 (dashed curve), 633 (dotted curve), and 919 (solid curve) nm.
(B) Kinetics of Bi:RbPb₂Cl₅ luminescence measured under 808 nm excitation and the exponential approximation.
Reproduced with permission (Okhrimchuk et al., 2008). Copyright 2008, Optical Society of America.
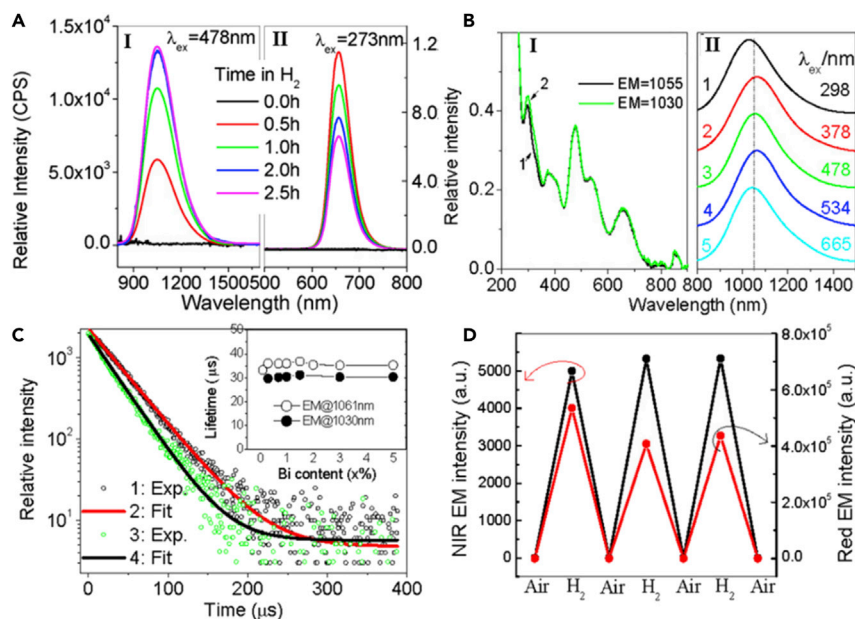
Figure 5. Luminescent Properties of Bi:Ba₂B₅O₉Cl

(A) (I, λ_{ex} = 478 nm) NIR and (II, λ_{ex} = 273 nm) red emission spectra of $Ba_{2(1-x)}B_5O_9Cl$: 2x%Bi (x = 0.3) treated in H_2 at 850°C for different times: black line, 0.0 h; red line, 0.5 h; green line, 1.0 h; blue line, 2.0 h; and pink line, 2.5 h.

(B) (I) Excitation (curve 1: λ_{em} = 1,055 nm; 2: λ_{em} = 1,030 nm) and (II) emission spectra (1: λ_{ex} = 298 nm; 2: λ_{ex} = 378 nm; 3: λ_{ex} = 478 nm; 4: λ_{ex} = 534 nm; 5: λ_{ex} = 665 nm) of $Ba_{2(1-x)}B_5O_9Cl$: 2x%Bi (x = 0.7).

(C) Decay and fit (with simple exponential decay equation) curves of $Ba_{2(1-x)}B_5O_9Cl$: 2x%Bi (x = 0.7): (1) and (2) for the case of the emission at 1,061 nm upon 478 nm excitation, and (3) and (4) for the emission at 1,030 nm upon the excitation of 298 nm. Inset shows the dependence of lifetime on the bismuth content x%.

(D) Reversely removing and recovering NIR (- ● -, λ_{ex} = 478 nm) and red (- ● -, λ_{ex} = 273 nm) emission centers of bismuth by repeatedly treating $Ba_{2(1-x)}B_5O_9Cl$: 2x%Bi (x = 0.3) in air and H_2 in turn. The emission was excited by 478 nm. Reproduced with permission (Peng et al., 2010). Copyright 2010, Optical Society of America.

had first considered Bi^0 as NIR origin in $Ba_2P_2O_7$ before this work (Peng et al., 2010), the introduction of Bi^0 into Bi-doped NIR luminescent chlorides should be an important leap. First, samples of $Ba_{2(1-x)}B_5O_9Cl$:2x% sintered under air showed no NIR emission. However, after treatment under N_2/H_2 reductive atmosphere, NIR PL peaked at 1,055 nm and the best duration time was confirmed as 2.5 h (Figure 5A). When monitored at 1,055 or 1,030 nm, similar well-separated excitation peaks at 298, 478, 665, and 850 nm were observed, and shoulder bands at ~ 378 and ~534 nm were also traced (Figure 5BI). The PL emission with FWHMs larger than 200 nm also were dependent on the excitation wavelengths (Figure 5BII). From these spectroscopic data, at least two emission centers were confirmed, which should result in two different Ba^{2+} sites described in XRD and Rietveld refinement. Lifetimes of emissions at 1,030 and 1,061 nm showed no clear dependence on Bi contents, and the lifetimes of 1,030 nm emissions (λ_{ex} = 298 nm) are between 29.63 and 31.16 μs, compared with that of 33.21–36.88 μs of 1,061 nm (λ_{ex} = 478 nm) (Figure 5C). Finally, if Bi:Ba₂B₅O₉Cl was alternatively treated in air and H_2/N_2, red emission and NIR emission centers can be removed and restored reversibly (Figure 5D). In all, these data demonstrated that Bi^0 should be the NIR origin in this compound.

However, they deepened their understandings of the nature of NIR Bi centers in this compound in 2016. They believed that the conversion of Bi^{2+} to Bi^0 happens via an intermediate state of Bi^+, which luminescence covers from 600 to 1,200 nm with a lifetime longer than 1 ms if stabilized on Ba^{2+} sites (Zheng et al., 2016). Upon 330 nm excitation, broad emission spectra (600–850 nm) peaked at 660 and 790 nm were observed (Figure 6A). Another peak centered at 970 nm can also be found (Figure 6B). The excitation spectra of peak 790 nm were depicted (Figure 6C). Two new strong peaks at 330 and 606 nm together with weak peak at 478 nm from Bi^0 were observed, whereas excitation spectrum of peak 970 nm just consists of two strong peaks at ~320 and ~670 nm. Finally, by comparing the lifetimes of each emission peak (Figure 6D), a dynamic conversion from Bi^{2+} to Bi^0 via Bi^+ was confirmed, and Bi^+ ions were confirmed after

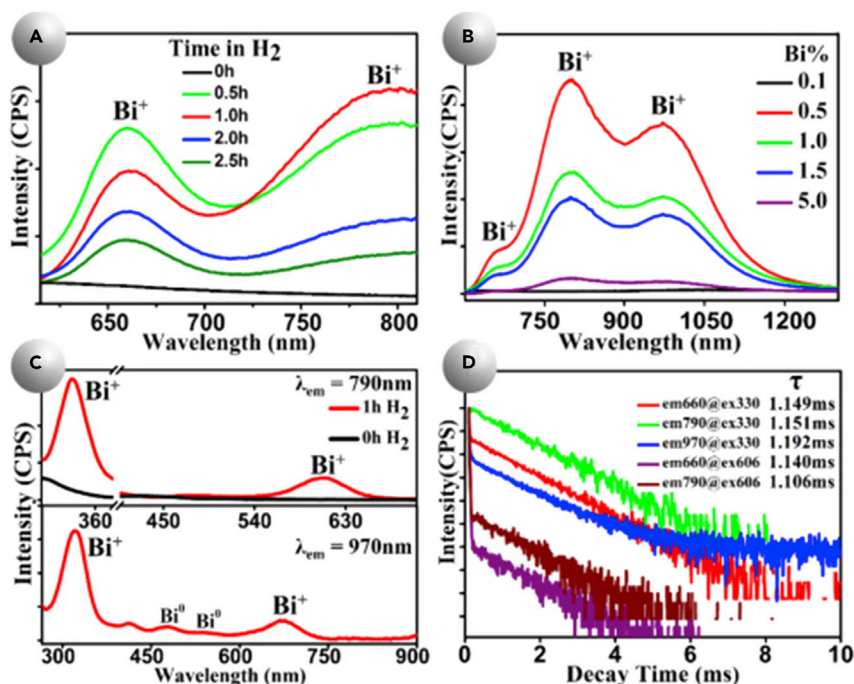**Figure 6. NIR Emissions of Bi:Ba₂B₅O₉Cl**

(A–D) (A) Emission spectra (λ_{ex} = 330 nm) of $Ba_{1.99}B_5O_9Cl$: 1%Bi treated in N_2/H_2 for different times; (B) emission spectra (λ_{ex} = 330 nm) of $Ba_{2(1-x\%)}B_5O_9Cl$: 2x%Bi (x = 0.1, 0.5, 1.0, 1.5, 5.0) treated in N_2/H_2 for 1 h detected by visible and NIR photomultipliers. The spectra were rescaled and combined. (C) Excitation spectra (λ_{em} = 790 nm, λ_{em} = 970 nm) of $Ba_{1.99}B_5O_9Cl$: 1%Bi treated in N_2/H_2 for 1 h and 0 h; (D) decay curves of $Ba_{1.99}B_5O_9Cl$: 1%Bi treated in H_2/N_2 for 1 h. Reproduced with permission (Zheng et al., 2016). Copyright 2016, Optical Society of America.

further discussion with other previous work. Also in 2012, Bi-doped NIR luminescence occurring in polycrystalline $Ba_{10}(PO_4)_6Cl_2$ was found by Li et al. (Li et al., 2012). They proposed that NIR emission peaked at ~ 1,250 nm under excitation of a 690-nm laser diode should come from Bi^+ ions, but further experimental data such as decay lifetime were missed. At that same age, Russian researchers began to focus on Bi-doped NIR luminescent chloride crystals in 2012; for example, Romanov et al. observed intense NIR emission in Bi-doped $KAlCl_4$ polycrystalline (Veber et al., 2012). They did this work because of the previous failed attempt in obtaining a medium with a single luminescent center in $ZnCl_2$-$AlCl_3$ glasses (Romanov et al., 2012). At room temperature, NIR PL centered at 975 nm with FWHM of 130 nm was observed. After cooling to 77 K, the peak blue shifts to 900 nm and the FWHM turns to 70 nm. In all, only one luminescent center exists in this system, and the reason for emission broadening is electron-phonon interaction. For the nature of NIR center, they agreed that Bi^+ should be responsible for the NIR emission, and they again confirmed this hypothesis by studying the NIR luminescent properties in ternary halide crystals $KAlCl_4$ and $KMgCl_3$ (Romanov et al., 2013). In 2013, Plotnichenko et al. thought that Bi^+ ions could easily substitute Tl^+ or Pb^+ ions in most crystalline halides, and they succeeded in obtaining two NIR bands with a lifetime of 0.25 ms: one strong band peaked at 1,180 nm excited by 400, 450, 700, or 800 nm wavelengths and a shoulder peak >1,500 nm under excitation of 400- and 450-nm lights. As for the NIR origin, Bi^+ ... V_{Cl}^- complexes formed by substitutional ions and intrinsic defects were confirmed. Soon afterward, Plotnichenko et al. demonstrated that Bi-doped AgCl crystals also could possess NIR emission (Figure 7); the PL band was in 800–1,200 nm range with two exponential component lifetimes of 1.2 and 10.3 μs excited mainly by 390–440 nm radiation. Together with the modeling results in this work, the main contribution to the NIR PL in Bi:AgCl was made by Bi^+ ions.

Some Bi-doped NIR crystals were found by accident; for example, in 2013, Li et al. intended to systematically study the effects of apatite structure on spectroscopic properties of alkaline earth metal chlorophosphate $M_5(PO_4)_3Cl$ (M = Ca, Sr, and Ba, MCAP) under air and reducing atmosphere, and they found that all samples emitted in the visible range from Bi^{3+} ions (Figure 8A), whereas $Ba_5(PO_4)_3Cl$ showed another NIR
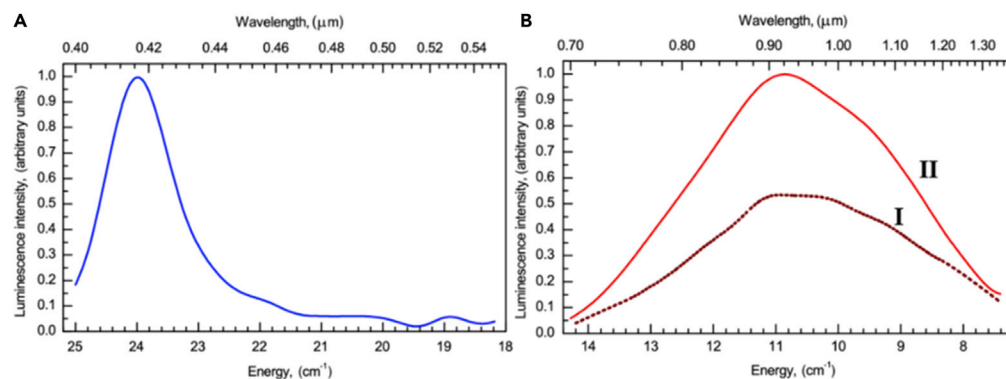
Figure 7. PL Properties of Bi:AgCl
(A) PLE spectrum of 0.90 μm luminescence in AgCl sample doped with metal Bi.
(B) PL spectra excited at 0.42 μm wavelength: (I) AgCl doped with Bi chloride and (II) AgCl doped with metal Bi.
Reproduced with permission (Plotnichenko et al., 2013). Copyright 2013, Optical Society of America.

band (Figure 8B) (Li et al., 2013). Based on the previous work and the principles of charge/radii match, Bi^{3+} ions were believed to be introduced into two different Ba^{2+} sites and only in $Ba^{2+}(1)$ sites can then be reduced to Bi^+ to feature NIR luminescence.

In 2014, Romanov et al. used Bridgman method to prepare Bi-doped single crystal of triple chloride $CsCdCl_3$ and realized its NIR emission of Bi^+ impurity (Romanov et al., 2014). The $CsCdCl_3$ host was chosen because it contains Cs^+, which can be substituted by Bi^+ ions. The NIR PL excitation spectra monitored at 993 nm showed two peaked orange-red bands centered at ~610 and 650 nm (Figure 9A), and the corresponding PL spectra under excitation by 615 nm irradiation showed peak at ~980 nm at room temperature (Figure 9B). One can clearly note that both the PL excitation and PL spectra were related to the surrounding temperatures. The existence of doubly degenerate E states of Bi^+ ion was the result of high symmetry, and the absorption spectra of Bi^+ comes from one/several transitions of A→E type. In 2016, Bi-doped NIR luminescent KCl using the Bridgman method was found to emit in the NIR range after γ-irradiated treatment by Firstov et al. (2016). The NIR emission peaks red shifted from 1,100 to 1,300 nm when the Bi content is decreased from 0.1 to 0.01 at.%, and this phenomenon may be due to the lattice distortion caused by increased Bi concentration. The typical lifetime is in the range of ~10–20 μs. They suggested that Bi^{2+} ion next to an anion vacancy was a possible NIR active center. Further in the same year, 2016, Romanov et al. prepared and found Bi-doped NIR luminescent single crystal of RbY_2Cl_7 ternary chloride (Romanov et al., 2016). The Bi^+ ions substituted for Rb cations whose position was characterized at a C_s symmetry
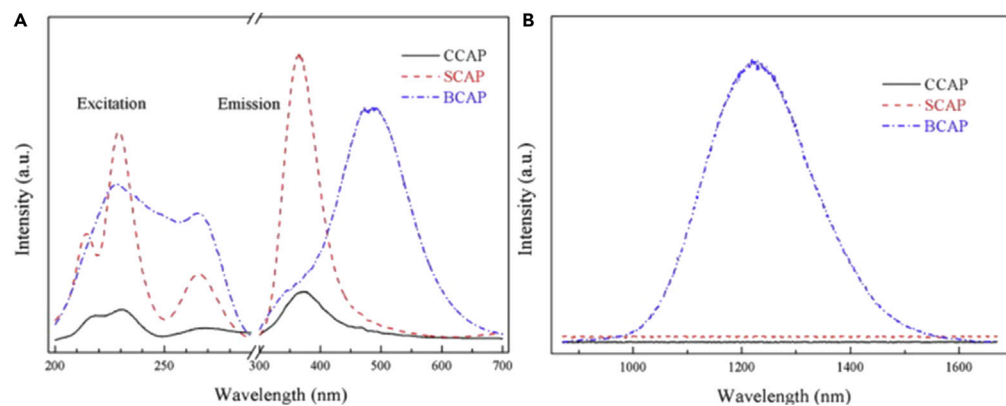

Figure 8. NIR PL Luminescent Properties of Bi:MCAP
(A) Normalized excitation and emission spectra of Bi-doped MCAP synthesized in the reducing condition.
(B) NIR luminescence spectra of the reduced-MCAP: Bi samples under excitation of 690-nm laser diode. Reproduced with permission (Li et al., 2013). Copyright 2013, Elsevier.
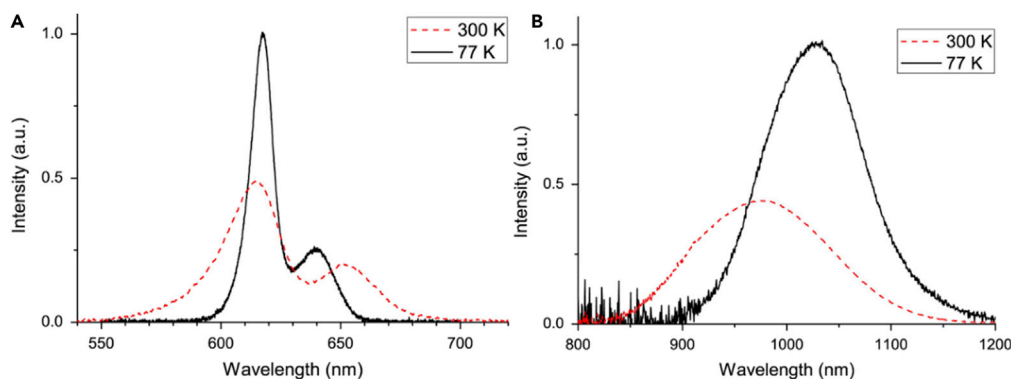
Figure 9. NIR Luminescent Properties of Bi:CsCdCl$_3$

(A) NIR PL excitation spectra for Bi$^+$-doped CsCdCl$_3$ single crystal (registered at 77 K and room temperature, luminescence registration at 993 nm).

(B) NIR photoluminescence spectra for Bi$^+$-doped CsCdCl$_3$ single crystal (registered at 77 K and room temperature, 615 nm excitation wavelength). Reproduced with permission (Romanov et al., 2014). Copyright 2014, Elsevier.

point group. Consequently, a single NIR optically active center of Bi$^+$ was expected, and this had been confirmed by its single exponential decay lifetime of 467 ms at room temperature. Worth noting, also in 2016, Vtyurina et al. systematically studied the spectral properties and NIR PL of Bi$^+$-doped triple chlorides such as RbAlCl$_4$, CsAlCl$_4$, RbMgCl$_3$, CsMgCl$_3$, KCdCl$_3$, and RbCdCl$_3$ (Vtyurina et al., 2016). First, all these triple chlorides were prepared by crystallization from the Lewis acidic melts. Meanwhile, broadband and long-lived NIR PL centered at ~ 1,000 nm was recorded from all systems (Figure 10). The most possible NIR origin here was considered as Bi$^+$ ions, whose substituted sites were large alkali cations such as K$^+$, Cs$^+$, and Rb$^+$. In this work, the authors insisted that group theory was a valid tool for the initial consideration of crystal field influence on those excited states of Bi$^+$ ions in different hosts, and they did calculate the crystal field splitting of the lowest electronic states in P^2 configuration. Moreover, they also roughly listed the factors of crystal system, space group, and point symmetry group at alkali ion position, and this should be a useful introduction for rationally designing Bi-doped NIR luminescent crystals. Unfortunately, one can find few work focused on Bi-doped NIR luminescent chlorides until 2019 when Peng et al. reported on a novel Bi-doped crystal Sr$_2$B$_5$O$_9$Cl with ultra-broadband emission covering the entire NIR range (780–1,600 nm) (Wang et al., 2019). It was necessary to reduce Bi^{3+} first under a H$_2$/N$_2$ atmosphere to obtain NIR emission (Figure 11A). And one can note that each broadband PL spectrum could be well decomposed into three emission bands centered at 780, 990, and 1,280 nm, respectively (Figure 11B), which indicated that more NIR centers were created after reducing treatment. Furthermore, the number of NIR centers were confirmed as three from the PL excitation spectra (Figure 11C). And due to the existence of multiple NIR Bi active centers, the PL emission could be widely tuned to cover the whole NIR region by choosing proper excitation wavelengths (Figure 11D). Based on the different dependence of NIR peak intensities of 990 and 1,280 nm on reducing time, at least two different NIR centers accounted for the two PL bands (Figures 11E and 11F). Furthermore, by strictly comparing the lifetimes of peaks of 990 and 1,280 nm, they concluded that different centers or one center in different valences may be the reason (Figure 12). Also, the dynamic conversion of Bi^{3+} into low valences such as Bi^{2+}, Bi$^+$, and Bi^0 may exist always, and this would lead to the special NIR luminescent properties of Bi in Sr$_2$B$_5$O$_9$Cl.

Bromides

Inspired by the design of Bi$^+$:CsCdCl$_3$, the first ternary bromide phase CsCdBr$_3$ was prepared and confirmed to provide an NIR Bi center by Romanov et al. in 2015 (Romanov et al., 2015b). The single crystal was prepared by Bridgman method, and Bi$^+$ ions were considered as the NIR center that peaked at ~ 1,053 nm. Under the excitation of green and red spectral ranges (λ_{ex} = 532, 635, 660, or 690 nm), an intense broadband NIR PL was observed. The PL shape and position of its maximum are independent of the excitation wavelength (Figures 13A and 13B). Within the whole PL band, temporal decay plot shows that the decay is single exponential, and the decay time τ is nearly unchanged (250 $\pm$ 6 µs) even when the PL wavelength is tuned from 970 to 1,250 nm (Figure 13C). Before this work, the luminescent properties of Bi-doped CsCdBr$_3$ were studied by Wolfert and Blasse (1984). Contrary to the preparation process of
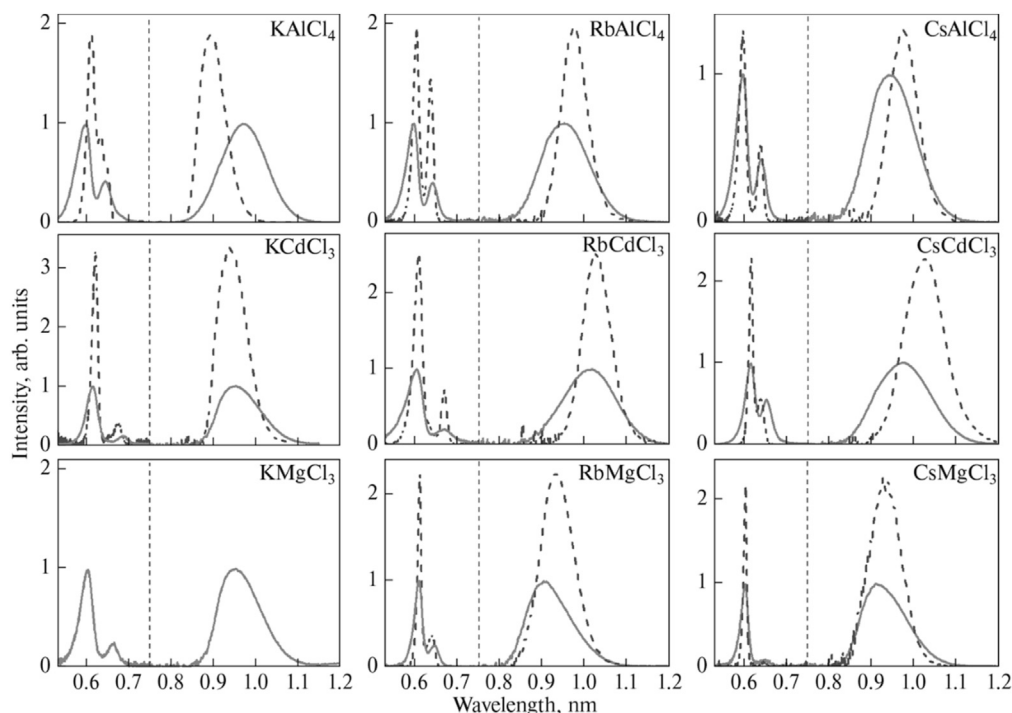
Figure 10. Luminescent Properties of Bi:AMCl_n

The photoluminescence excitation (0.53–0.75 μm) and emission spectra (0.75–1.2 μm) of the Bi$^+$-doped AMCl$_n$ (A = K, Rb, Cs; M = Al, Mg, Cd) crystal phases at 300 K (solid lines) and 77 K (dashed lines). The data for bismuth-doped KAlCl$_4$, KMgCl$_3$, and CsCdCl$_3$ were reported previously, and the spectral properties are given for clarity only; the presented data are modified after Romanov et al. (2014, 2015a) and Veber et al. (2012) respectively. Reproduced with permission (Vtyurina et al., 2016). Copyright 2016, Pleiades.

using a reductive environment with an excess of Bi metal, they prepared samples under an oxidative atmosphere (an excess of bromine) to guarantee that all Bi ions enter the crystal phase as Bi^{3+}. Only one PL center with the excitation maximum at 4.33 eV (286 nm) and emission maximum at 2.12 eV (585 nm) was observed. This PL center was attributed to Bi^{3+} in Cd^{2+} position, and clearly this is not involved in NIR PL. Notably, the NIR luminescent properties in Bi-doped CsCdBr$_3$ closely resemble those in CsCdCl$_3$, and the maximum in PL spectra and two maxima in PL excitation spectra are all red shifted. These results also indicate that the substitution of chloride ions by bromide ones in Bi$^+$-related environment would reduce the energies of sublevels of $^3P_1$ and $^3P_2$ manifolds.

Iodides

Besides, one can also obtain NIR emission from Bi-doped iodides such as in CsI (Su et al., 2011), TlCdI$_3$ (Romanov et al., 2017), and CsPbI$_3$ (Zhou et al., 2016). In 2011, Su et al. observed two ultrabroadband NIR luminescence bands around 1,200 and 1,500 nm (excited by 808 nm light) in as-grown Bi-activated CsI halide crystals (Figure 14). The Bi:CsI crystal was grown by the temperature gradient technique using CsI and BiI$_3$ (0.2 mol%). As for the FWHM and lifetime at 1,216 nm, they are 170 nm and 0.13 ms, whereas 145 nm and 0.22 ms are observed at 1,560 nm. Here, they found that it is not necessary to produce NIR luminescent centers by additional treatment such as irradiation or heat annealing. One can also note two different NIR centers from the photoluminescence excitation (PLE) spectra in Figure 14A, but both of them should be single centers because of unchanged central wavelengths and shapes of two NIR emission bands (Figure 14B). Experimental results in this work comply with the hypothesis of Bi$^+$ as NIR center. Afterward in 2016, Zhou et al. demonstrated that Bi-doped CsPbI$_3$ polycrystalline powders can obtain NIR emission at ~ 1,185 nm with an FWHM of 175 nm and a lifetime of tens of microseconds. However, they insisted on the fact that polaronic defects rather than single Bi center should account for NIR PL in this system, defects that can also be created by the incorporation of tellurium. In this system, they believed that two points are required to be addressed: first, the characteristic lifetimes are in the range of tens of
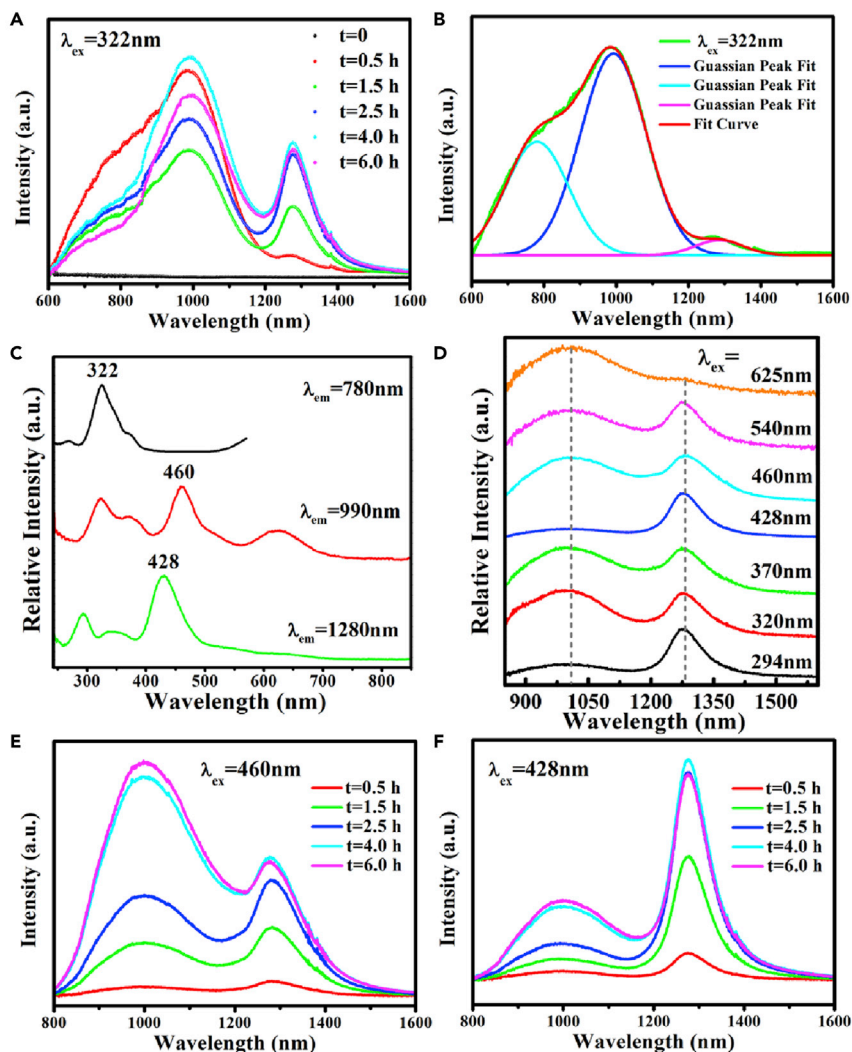
Figure 11. PL Luminescent Properties of Bi:Sr$_2$B$_5$O$_9$Cl

(A) Emission spectra (λ_{ex} = 322 nm) of Sr$_{2(1-x)}$B$_5$O$_9$Cl:2xBi (x = 1.0%) treated in N$_2$/H$_2$ for different times.

(B) The Gaussian peak decomposition results corresponding to λ_{ex} = 322 nm, t = 0.5 h).

(C) Excitation spectra of Sr$_{2(1-x)}$B$_5$O$_9$Cl:2xBi (x = 1.0%), treated in t = 0.5 h.

(D–F) (D) Emission spectra of Sr$_{2(1-x)}$B$_5$O$_9$Cl:2xBi (x = 1.0%) excited by light with wavelengths from 294 nm to 625 nm. Emission spectra at (E) λ_{ex} = 460 nm and (F) λ_{ex} = 428 nm of Sr$_{2(1-x)}$B$_5$O$_9$Cl:2xBi (x = 1.0%) treated in N$_2$/H$_2$ for different times. Reproduced with permission (Wang et al., 2019). Copyright 2019, Optical Society of America.

micro-seconds, and second, more free electrons can be obtained after doping Bi ions. And based on the two facts, they offered a structure model to explain the source of NIR PL (Figure 15). The structure modification from the replacement of Pb^{2+} by Bi^{3+} will create non-spin paired (s = 1/2) polarons with g value similar to that of free electrons, and this will induce in-gap optical active states in the band gap, which results in NIR PL (Figure 15A). Moreover, an energy level diagram of polaronic defect was provided based on the absorption and PL excitation spectra (Figure 15B), and this should provide more details about the process of NIR PL in Bi-doped CsPbI$_3$.

Since the widths of the band gap of the CsPbI$_3$ (3.14 eV) and TlCdI$_3$ (3.326 eV) crystals are comparable, one can expert similar NIR PL emission in Bi-doped TlCdI$_3$. In 2017, Romanov et al. found that Bi-doped single-crystal TlCdI$_3$ also can show NIR PL, which peaks at 1,175 nm. However, they believed that the main emitting center of Bi:TlCdI$_3$ is Bi^{2+}, although its PL spectra is significantly different from the Bi^{2+} emissions in other materials. One can clearly note that a redshift occurs from visible to NIR range compared with that in other
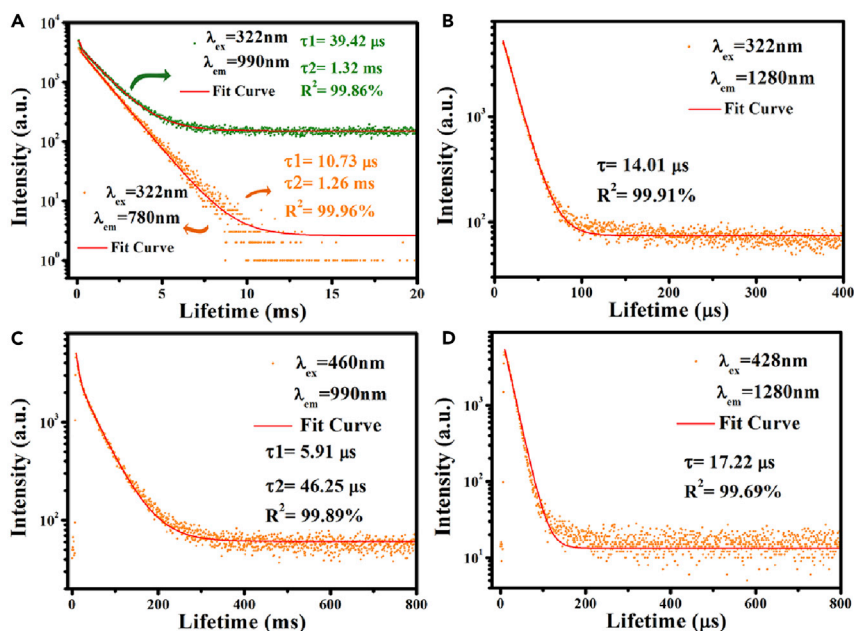
Figure 12. Decay Properties of Bi:Sr$_2$B$_5$O$_9$Cl

(A–D) Decay and fitting curves of Sr$_{2(1-x)}$B$_5$O$_9$Cl:2xBi (x = 1.0%): (A) for the case of λ_{ex} = 322 nm, λ_{em} = 780 nm and λ_{ex} = 322 nm λ_{em} = 990 nm, respectively, and (B) for the emission at 1,280 nm upon the excitation of 322 nm; (C) λ_{ex} = 460 nm, λ_{em} = 990 nm; and (D) λ_{ex} = 428 nm, λ_{em} = 1,280 nm. Reproduced with permission (Wang et al., 2019). Copyright 2019, Optical Society of America.

compounds, and this should be attributed to the interaction of the excited electronic states of the impurity center within the nearby located conduction band of TlCdI$_3$.

Oxide Compounds

Borates

In 1984, Blasse et al. first found that Bi-doped SrB$_4$O$_7$ can be used to realize unique orange-red lumines-cence of Bi^{2+} ions (Blasse et al., 1994). However, no reports had focused on its NIR emission in this host until 2005 when Peng et al. first obtained an NIR PL (peaked at ~1,260 nm) under excitation by an 808-nm laser light (Figure 16), and one should note that this was also the first NIR PL emission from Bi-doped crystals (Peng et al., 2007). At the first time, Peng et al. tried and succeeded in obtaining broadband PL (1,200–1,600 nm) from Bi-doped zinc aluminosilicate glasses and glass-ceramics. They found that with the content increase of nano-crystalline ZnAl$_2$O$_4$, the NIR PL intensities were decreased continuously. Usually, in the crystallizing course of glasses, the active ions will enter the crystalline phase, and therefore the lumines-cence intensity could be strongly enhanced in glass-ceramics. Hence, it seems that doped Bi ions still stay in the residual glass phase of the formed glass-ceramics, and the interaction between Bi ions becomes stronger because of the introduction of Al^{3+} ions, which finally weakens the NIR PL intensity. As for the source of NIR PL, Peng et al. first excluded the possibilities of high-valence Bi such as Bi^{5+} based on optical basicity calculation. When it comes to low-valence Bi ions, they chose SrB$_4$O$_7$ as the host because this com-pound was confirmed to possess strong reducing ability even when sintered in an oxidizing atmosphere. Finally, on excitation with 808 nm laser, a weak broadband PL (1,100–1,500 nm) was observed from Sr$_{0.95}$B$_4$O$_7$:0.05Bi, which indicates that low-valence Bi should account for the NIR emission. Afterward, researchers around the world began to focus on Bi-doped NIR crystals. In 2009, for SrB$_4$O$_7$ compound, Su et al. did systematic study on the spectroscopic properties of Bi-doped SrB$_4$O$_7$ glasses and crystalline materials (polycrystalline and single crystalline materials) (Su et al., 2009b). They found that both Bi-doped glass (Figure 17A) and polycrystalline (Figure 17B) possess NIR PL emission, whereas no NIR PL was observed in Bi:SrB$_4$O$_7$ single crystal. Although they had tried to reduce the valence of Bi in SrB$_4$O$_7$ single crystal by H$_2$ annealing and γ irradiation, no desired NIR PL was observed. This should be attributed to the three-dimensional network of SrB$_4$O$_7$ single crystal, which is too rigid to accommodate Bi$^+$ (1.45 Å) in Sr^{2+} site (1.12 Å).
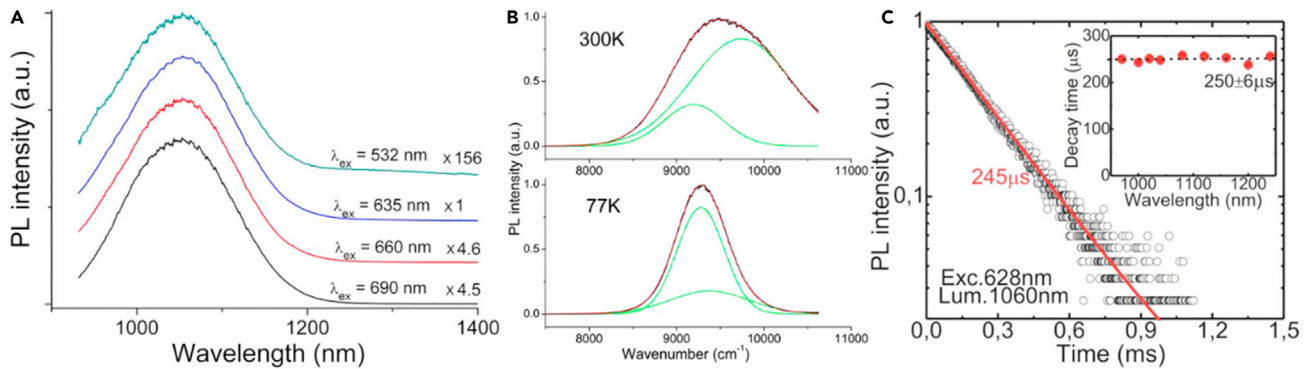
Figure 13. NIR Luminescent Properties of Bi:CsCdBr$_3$

(A) Photoluminescence emission spectra of Bi$^+$-doped CsCdBr$_3$, excited at different wavelengths (300 K).

(B) Photoluminescence emission spectra of Bi$^+$-doped CsCdBr$_3$ at 77 and 300 K; Gaussian decompositions (2 Gaussians) of both spectra are shown.

(C) Photoluminescence decay plot for Bi$^+$-doped CsCdBr$_3$ (excitation wavelength is 628 nm, PL wavelength is 1,060 nm); inset shows the dependence of characteristic decay time on the emission wavelength within the photoluminescence band. Reproduced with permission (Romanov et al., 2015b). Copyright 2015, Elsevier.

Compared with the three-dimensional [BO$_4$] network structure of SrB$_4$O$_7$ crystal, the quasistable phase of α-BaB$_2$O$_4$ with relatively relaxed lattice structure composed of two-dimensional [B$_3$O$_6$] triangles is appropriate for accommodating Bi$^+$ ions. Finally, the NIR PL was confirmed in α-BaB$_2$O$_4$ single crystal by Xu et al. (Su et al., 2009b; Xu et al., 2010). In 2009, they first investigated the spectroscopic properties of as-grown and γ-irradiated undoped and Bi-doped α-BBO (BaB$_2$O$_4$) single crystals. Broadband emission at 1,139 nm of γ-irradiated Bi: α-BBO crystal with an FWHM more than 100 nm and a lifetime of 520 μs can be obtained under 808 and 980 nm laser excitation (Figure 18). Meanwhile, Bi^{2+} and color centers were confirmed to be nonluminescent in the NIR region. So the most probable NIR center in γ-irradiated Bi: α-BBO should be Bi$^+$. They also studied the thermal stability of the NIR center (Bi$^+$), and results show that the broad absorption band at 748 nm, which relates to Bi$^+$, has nearly disappeared after annealing, and no NIR PL can be obtained. Thus, the trapped electrons in Bi$^+$ ions can be released by thermal activation.

In the next year, 2010, Xu et al. began to systematically study the effect of heat annealing (H$_2$, Ar, and air atmosphere) and irradiation (γ or electron irradiation) on luminescent properties of Bi: α-BBO single crystal. As for the influence of atmosphere, NIR PL with center wavelength of 985 nm and FWHM of 187 nm was only produced under H$_2$ atmosphere (Figure 19), and the decay time of 985 nm emission was measured to be 408 μs. For comparison, the peak wavelength, FWHM, and lifetime of γ irradiated Bi: α-BBO crystal were 1,140 nm, 108 nm, and 526 μs, respectively. From the absorption, excitation and NIR PL spectra of γ-irradiated and H$_2$-annealed Bi: α-BBO crystal in this work, the authors calculated the electronic energies of multiplets of
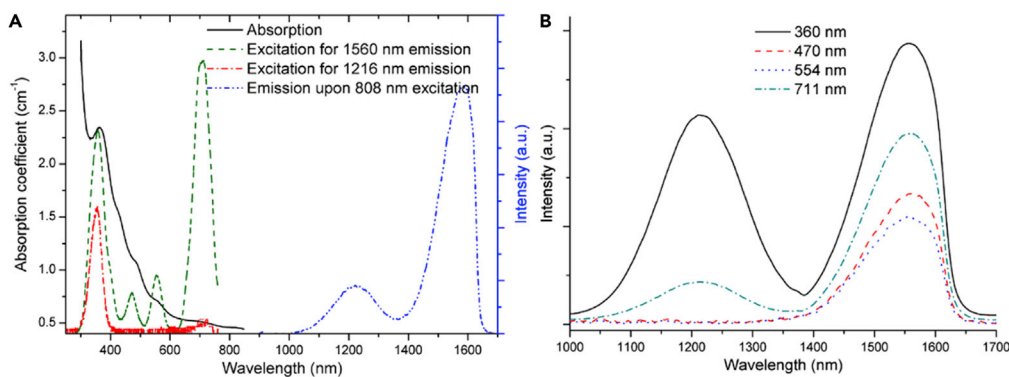

Figure 14. Luminescent Properties of Bi:CsI

(A) Absorption, emission, and corresponding excitation spectra of the as-grown 0.2 at.% Bi:CsI crystal at 300 K.

(B) NIR luminescence spectra of the Bi:CsI crystal at 300 K under excitation wavelengths of 360, 470, 554, and 711 nm. Reproduced with permission (Su et al., 2011). Copyright 2011, Optical Society of America.
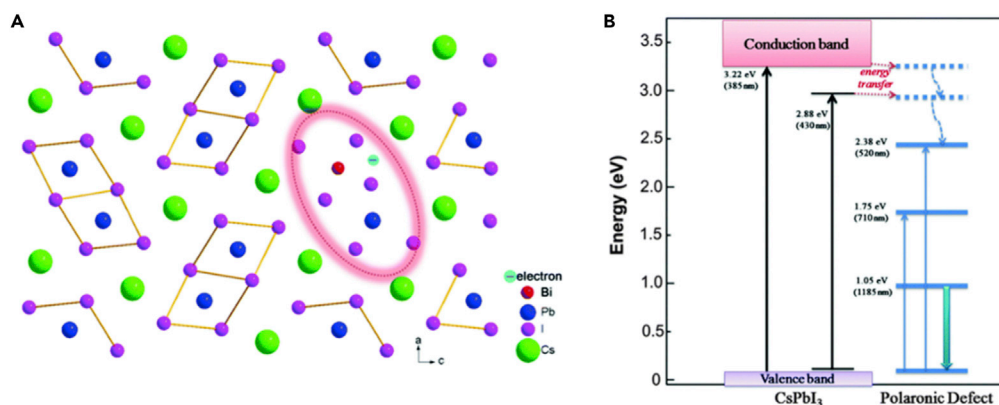
Figure 15. NIR Luminescent Properties of Bi:CsPbI₃

(A) Schematic illustration of Bi-doped $CsPbI_3$. The ellipse represents the luminescent polaronic defect induced by Bi incorporation.

(B) Relevant energy levels of Bi-doped $CsPbI_3$. The wavelengths and energies shown for transitions are experimentally determined based on the measurements of absorption, PL, and PL excitation spectra. Note that the dotted blue lines indicate the possible high energy levels of the luminescent polaronic defect. Reproduced with permission (Romanov et al., 2017). Copyright 2017, Pleiades.

the NIR centers and compared them with those of free Bi^+ ions. Thus, Bi^+ ions were confirmed as the NIR center. Worth pointing out, they also used electron beam to directly reduce Bi^{3+} to a low valence, and this finally gave success in obtaining an NIR emission with central wavelength of 1,131 nm and an FWHM of 98 nm.

Silicates

Bi-doped silicates such as $KGaSi_2O_6$ leucites also possess NIR PL. In 2014, Romanov et al. found that Bi-doped compositions of $20KGaSi_2O_6$-$1Bi_2O_3$ in both quenched clear glass and crystallized specimens can produce NIR emission (Figure 20A) (Romanov et al., 2015a). Upon glass crystallization, NIR PL peaks become much sharper and blue shift compared with glass sample. Two points can be considered to explain this phenomenon: first, the spectra become sharper after the NIR center transition from disordered (glass) to ordered (crystal) phase; second, glass samples contain many kinds of NIR Bi centers, but only a part of them can enter crystal phase, which finally simplifies the PL spectra. Here, Bi^+ isomorphically substituting for K^+ was suggested as NIR PL center and was confirmed by temporal decay spectra (Figure 20B). Clearly,
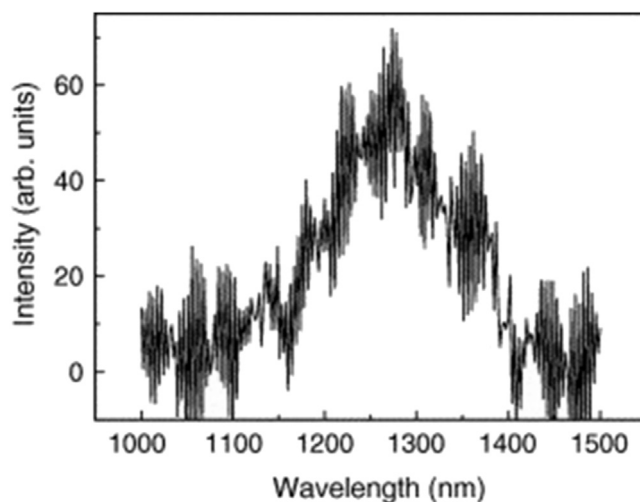

Figure 16. PL Spectrum of $Sr_{0.95}B_4O_7$:0.05Bi Prepared in Air when Pumped by 808-nm Laser Diode.
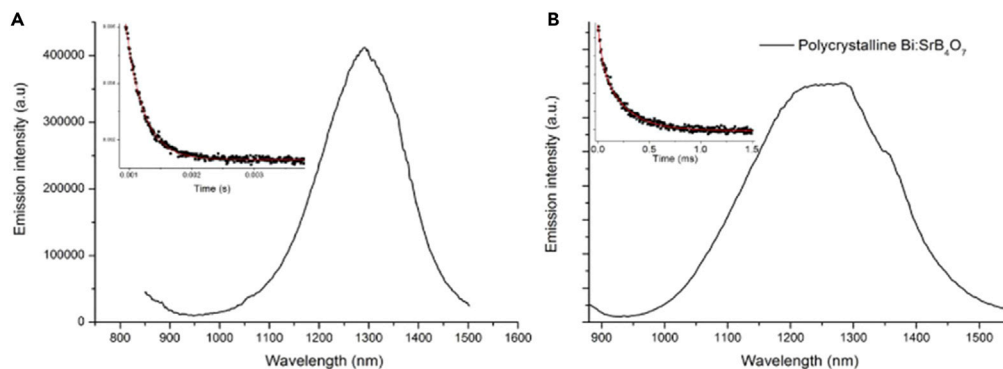Reproduced with permission (Peng et al., 2007). Copyright 2007, Elsevier.

Figure 17. NIR Luminescent Properties of Bi:SrB$_4$O$_7$

(A) NIR spectrum of the yellow Bi:SrB$_4$O$_7$ glass under 808-nm laser diode pumping. The inset is emission decay curve at 1,292 nm.

(B) NIR spectrum of polycrystalline Bi:SrB$_4$O$_7$. The inset is the decay curve at 1,290 nm. Reproduced with permission (Su et al., 2009b). Copyright 2009, Optical Society of America.

the decay spectra are always single exponential whose lifetimes only vary slightly (401–429 μs) along the wavelength range of 1,100–1,300 nm, and this is also similar to that of Bi$^+$ ions in other crystal. Also, a characteristic 2D excitation-emission plot was provided (Figure 20C); two well-distinguished branches of luminescent signals can be obtained.

Aluminates

An intense and broadband NIR (900–1,700 nm) PL emission was observed in Bi-doped mixed Gd$_{0.1}$Y$_{0.9}$AlO$_3$ single crystal grown by Czochralski method by Chen et al. in 2018 (Chen et al., 2018). Compared with YAlO$_3$ crystal, this mixed crystal can feature more substitutional sites, large ground state split, and disorder structure. In their work, broadband NIR spanning 900–1,700 can be observed under the excitation of 600 nm (Figure 21A), which is ascribed to Bi$^+$ ions. For comparison, Bi-undoped Gd$_{0.1}$Y$_{0.9}$AlO$_3$ sample shows no
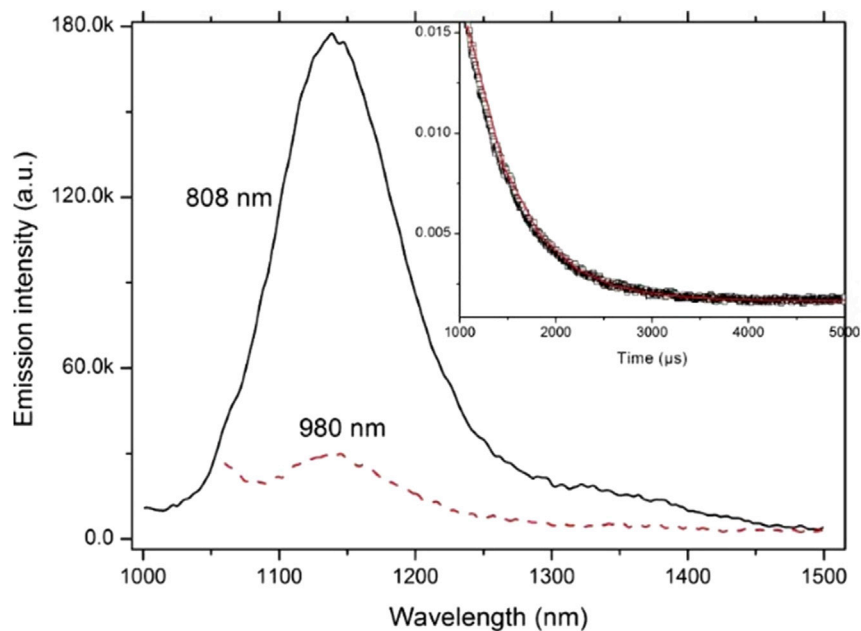

Figure 18. NIR PL Spectra of the γ-Irradiated Bi:α -BBO Crystal upon 808- and 980-nm Laser Diode Excitation, Respectively

The inset is the decay curve of the emission at 1,139 nm. Reproduced with permission (Su et al., 2009b). Copyright 2009, Optical Society of America.
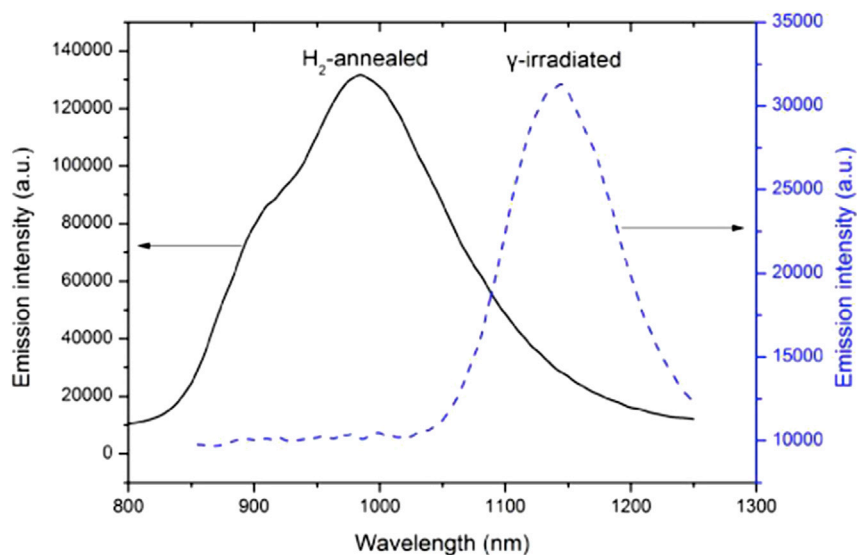
Figure 19. NIR Emission Spectra of H$_2$-Annealed and γ-Irradiated Bi:α-BaB$_2$O$_4$ Crystals under Excitation of 808-nm Laser Diode.
Reproduced with permission (Xu et al., 2010). Copyright 2010, Optical Society of America.

NIR PL at all. Decay lifetime of peak 1,080 nm was also confirmed to be 354.38 μs (Figure 21B). At least two NIR centers can be expected in Bi:Gd$_{0.1}$Y$_{0.9}$AlO$_3$ crystal, together with the super broad NIR band, this system may be used as tunable ultrashort laser medium materials.

Aluminum Silicates

The Bi-doped aluminosilicate phase leucite (KAlSi$_2$O$_6$) and pollucite (CsAlSi$_2$O$_6$) were confirmed to possess NIR PL by Romanov et al. (2015a). Optically active center is Bi$^+$ ions, which substitute for the alkali metal cations such as K$^+$ and Cs$^+$. Similar to that described in KGaSi$_2$O$_6$ leucites above, the NIR PL emission peaks in Bi-doped leucite (KAlSi$_2$O$_6$) also become much sharper and blue shift relative to the corresponding glasses (Figure 22A). They also successfully prepared Bi-doped pollucite, and due to the similar crystal structure to leucites, similar NIR emission was finally obtained under different excitation wavelengths (405, 532, 635, 660, and 690 nm) (Figure 22B). This result indicates that several NIR Bi centers co-exist in this system. And increased amount of Bi in the batch would lead to more Bi luminescent centers in pollucite (Figure 22C).

Phosphates

In 2010, Peng et al. first attributed the NIR Bi centers to Bi^0 in Ba$_2$P$_2$O$_7$ (Peng et al., 2010). First, they prepared three isomorphic crystal hosts of M$_2$P$_2$O$_7$ (M = Ca, Sr and Ba) to accommodate for Bi^{2+} and Bi$^+$ ions. However, NIR emission can only be obtained from Ba$_2$P$_2$O$_7$, centering at ~1,100 nm for an excitation wavelength of 723 nm (Figure 23A). The FWHM of this PL peak is 147 nm, which is narrower than those of most typical Bi-doped silicate and germanate glasses, but wider than that of α-BaB$_2$O$_4$ (108 nm) (Su et al., 2009b). Temporal decay agrees with a single exponential equation with a lifetime of 634 μs. From the uncorrected excitation spectra monitored at 1,100 μm, at least eight individual peaks at 586, 700, 723, 838, 900, 924, 955, and 997 nm were observed (Figure 23B). Compared with glass hosts, the much sharper excitation peaks come from the result that Bi was introduced into highly localized lattice sites, and additional excitation bands should be related to Bi on more than one site. As discussed by Peng et al. before this work (Peng et al., 2009), they believed that atomic spectral data of Bi^0 show the best consistence with spectroscopic data of Bi-doped glasses and crystals. Comparing the known radius of possible Bi species and calculating the relative ionic radius difference, they finally agreed that Bi^0 species can be accommodated in Ba$_2$P$_2$O$_7$ lattice to feature NIR emission but not in Ca$_2$P$_2$O$_7$ or Sr$_2$P$_2$O$_7$.
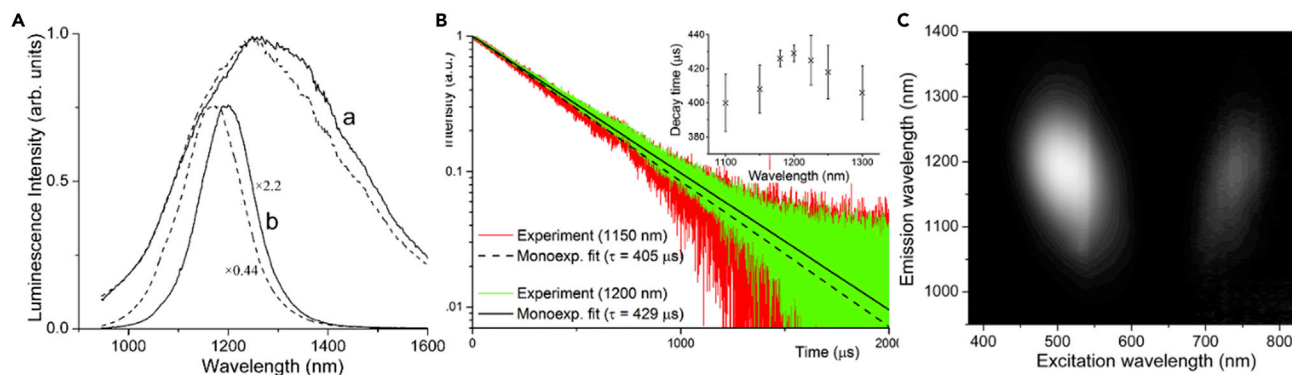
Figure 20. NIR Luminescent Properties of $20KGaSi_2O_6$-$1Bi_2O_3$ Glass

(A) PL spectra of the $20KGaSi_2O_6$-$1Bi_2O_3$ glass before (a) and after (b) crystallization. PL was excited at 470 nm (solid line) and 532 nm (dashed line). The scaling factors for the spectra of crystallized specimens are given relative to the spectra of glass, excited at the same wavelength.

(B) PL decay plots for the Bi-doped $KGaSi_2O_6$ specimen, registered at 1,150 and 1,200 nm (λ_{ex} = 532 nm). The characteristic decay times, measured at seven different wavelengths, are shown in the inset.

(C) The dependence of the NIR PL intensity on the PLE wavelength for the Bi-doped $KGaSi_2O_6$ specimen. White color means brighter emission. Reproduced with permission (Romanov et al., 2015a). Copyright 2010, The Royal Society of Chemistry.

In 2016, Liu et al. realized another Bi-doped NIR luminescent phosphate crystal of $BaBPO_5$ by converting Bi-doped red-emitting systems (Liu et al., 2016). From detailed analysis of X-ray absorption data, the introduced Bi ions should exist mostly in P^{5+} and/or B^{3+} sites, whereas a minority of them are located in Ba^{2+} lattice sites. Subsequent so-called topotactic reduction using Al powder would result in defective BiO polyhedral where Bi ions are in a lower valence (<3), and NIR emission was obtained. In Bi:$BaBPO_5$ precursor, red PL band centered at 642 nm corresponding to the $^3P_{3/2}(1) \rightarrow {}^2P_{1/2}$ transition of Bi^{2+} was detected (Figure 24A). Clearly, the thermal treatment of precursor has greatly weakened red PL, accompanied by the appearance of NIR PL band peaked at ~ 1,164 nm excited by 476 nm (Figure 24B). Furthermore, the excitation-emission gap of sample BBPO@450-3 demonstrates two peaks corresponding to the PL/PLE wavelengths of 1,160/476 and 1,120/700 nm (Figure 24C). These data indicate that NIR emission should come from at least two classes of optically active center. Meanwhile, multi-exponential decay was confirmed from the time-resolved PL spectra, leading to the effective lifetimes at 1,164 nm within the range of 81–116 μs. This work anticipated that low-temperature topotactic reduction strategy could be used to exploit more novel Bi-doped NIR luminescent crystals.
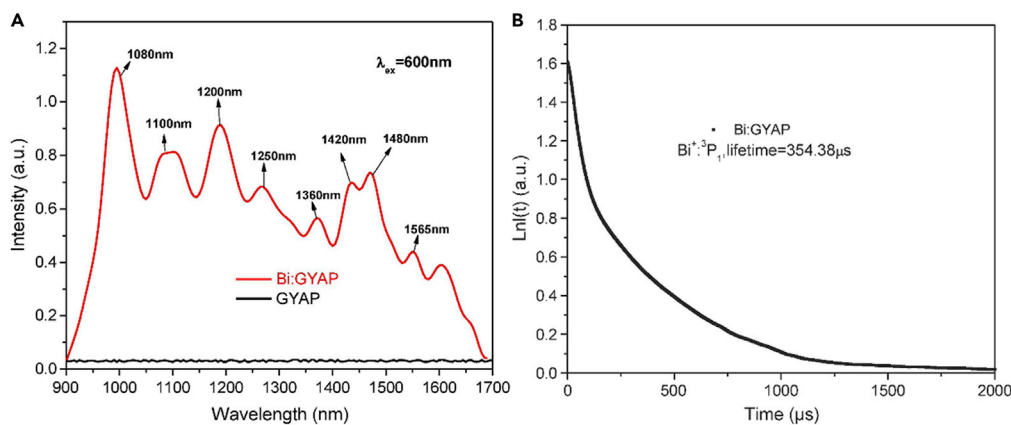

Figure 21. Luminescent Properties of Bi Doped Aluminates

(A) NIR emission spectra of Bi: $Gd_{0.1}Y_{0.9}AlO_3$ (Bi:GYAP) crystal under excitation of 600 nm.

(B) The decay time of the NIR emission band at 1,080 nm of Bi: $Gd_{0.1}Y_{0.9}AlO_3$. Reproduced with permission (Chen et al., 2018a). Copyright 2018, Elsevier.
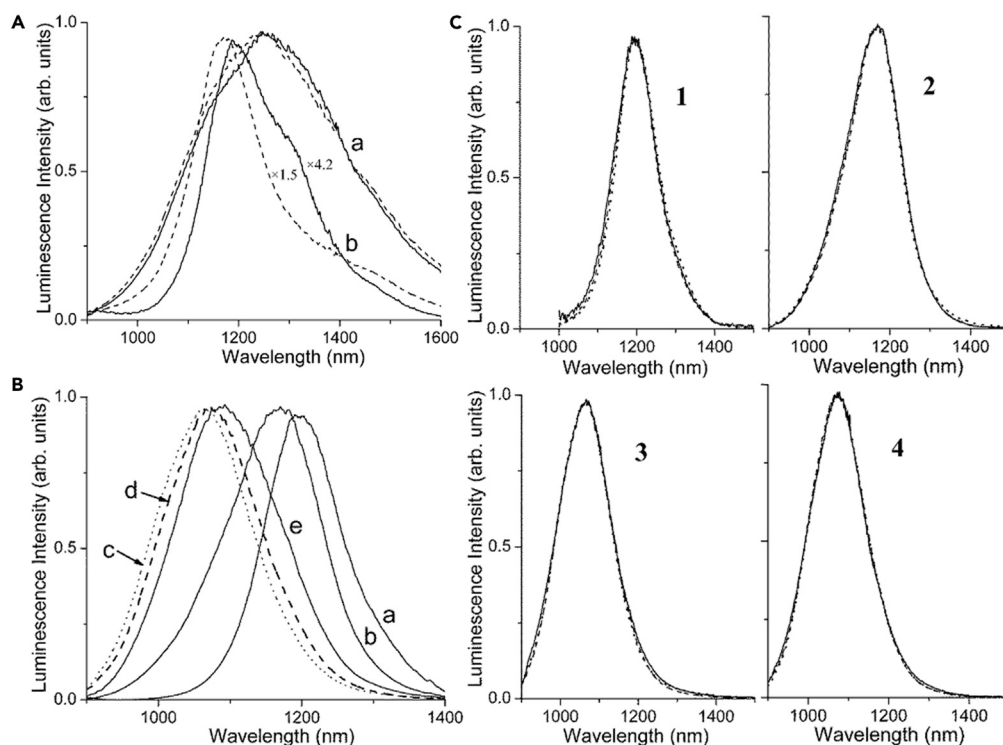
Figure 22. NIR Luminescent Properties of Bi Doped Aluminum Silicates

(A) PL spectra of the $60KAlSi_2O_6$-$40MgCaSi_2O_6$-$5Bi$ glass before (a) and after (b) crystallization. PL was excited at 470 nm (solid line) and 532 nm (dashed line). The scaling factors for the spectra of crystallized specimens are given relative to the spectra of glass, excited at the same wavelength.

(B) PL spectra of Bi-doped pollucite, crystallized from the melt with $7CsAlSi_2O_6$-$3B_2O_3$-$1.05Bi_2O_3$ composition. The luminescence was excited at (a) 405 nm, (b) 532 nm, (c) 635 nm, (d) 660 nm, and (e) 690 nm.

(C) PL spectra comparison for the Bi-doped pollucite samples, crystallized from the melts with $7CsAlSi_2O_6$-$3B_2O_3$-xBi_2O_3 compositions, containing different bismuth oxide amounts (for the solid line $x = 0.117$; for the dashed line $x = 0.35$; and for the dotted line $x = 1.05$). The luminescence was excited at 405 nm (1), 532 nm (2), 635 nm (3) and 660 nm (4). The intensity was scaled to superimpose the spectra upon one another. Reproduced with permission (Romanov et al., 2015a). Copyright 2010, The Royal Society of Chemistry.

Tungstates

In 2012, Xiong et al. prepared Yb/Bi co-doped PWO ($PbWO_4$) crystal, which exhibited two isolated emission peaks at 1,360 nm and 1,570 nm under 940 nm excitation (Xiong et al., 2012). One can see from Figure 25A that 1,360-nm and 1,570-nm peaks are much weaker than 1,060-nm peak (originates from Pb vacancy). NIR was observed in Bi-doped and Yb/Bi co-doped samples excited under 940 nm. They suggested these two isolate NIR peaks be ascribed to Bi^+, which was produced under reducing atmosphere caused by almost sealed crucibles. Yb^{3+} ions act as sensitizer due to the better gap matching between Yb^{3+} (from $^2F_{7/2}$ to $^2F_{5/2}$) and Bi^+ (from $^3P_2, ^3P_1$ to $^3P_0$), as can be seen in Figure 25B.

Germanates

Broadband NIR centered at 1,155 nm was achieved in Bi-doped Y_4GeO_8 crystal in 2011 by Xu and co-workers (Xu et al., 2011). Similar to previous work of Bi-doped α-BaB_2O_4 single crystal (Su et al., 2009a; Xu et al., 2010), γ-ray irradiation plays an essential role in NIR luminescence. In Figure 26, samples are described as XA, XR, or XRT, where X represents the concentration of Bi in mol. %. A, R, and T represent sintered in air, irradiation, and heat treatment temperature, respectively. It can be seen that the unirradiated sample did not exhibit NIR emission. The author suggested that free electrons and holes were generated and then captured by Bi^{3+} after γ-ray irradiation. Lower-valence Bi species were then generated, leading to the appearance of NIR and decrease of emission intensity of Bi^{3+}. When the irradiated samples were further treated under different temperature, the electrons and holes captured by Bi^{3+} release and
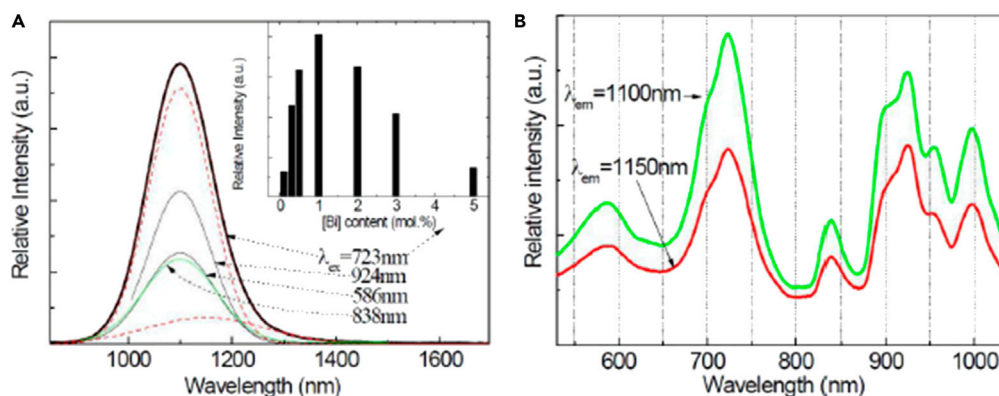
Figure 23. Luminescent Properties of Bi:M$_2$P$_2$O$_7$
(A) NIR emission spectra of Ba10A excited at 586 nm, 723 nm (dotted lines: Gaussian peak fits), 838 nm, and 924 nm, and dependence of NIR emission intensity on nominal bismuth concentration (inset).
(B) Uncorrected excitation spectra of Ba10A for emission at 1,100 and 1,150 nm, respectively. Reproduced with permission (Peng et al., 2010). Copyright 2010, Optical Society of America.

recombine with each other, leading to the increase of relevant Bi^{3+} emission and the decrease of NIR luminescence.

Recently in 2019, broadband NIR was achieved in bismuth-doped pollucite-related structure CsGaGe$_2$O$_6$ crystal (Romanov et al., 2019). The samples were crystallized from melt and then quenched in cold water. To remove the remaining glassy phase, the samples were etched on KOH solution. Bi-doped CsGaGe$_2$O$_6$ crystal exhibits similar NIR PL spectra as Bi-doped CsAlSi$_2$O$_6$ crystal (Romanov et al., 2015a), although the NIR PL spectra of the former is somewhat red shifted. Furthermore, the dependency of Bi-doped CsGaGe$_2$O$_6$ NIR PL emission spectra on excitation wavelength (Figure 27) is also consistent with Bi-doped CsAlSi$_2$O$_6$. The author ascribed Bi$^+$ monocation on Cs$^+$ site as NIR emission center in the as-prepared crystal. It was worth noting that NIR emission was observed in gallium excess sample (1:1.054CsGaGe$_2$O$_6$:Bi) rather than standard stoichiometric sample (1:1CsGaGe$_2$O$_6$:Bi). This can be explained considering the role of oxoacidity in the formation and stabilization of subvalent bismuth monocation in the melt. Bi^{3+} ions will be reduced to Bi$^+$ during thermal dissociation, and basic O^{2-} released at the same time: Bi$_2$O$_3$ $\leftrightarrow$ 2Bi$^+$ +O^{2-} +O$_2\uparrow$. Taking aggregation of Bi$^+$ into consideration: 6nBi$^+$ +3nO^{2-} $\leftrightarrow$ nBi$_2$O$_3$ + 4Bi$_n$. One can easily understand that low basic O^{2-} concentration (high oxoacidity) of the melt helps to form and stabilize Bi$^+$. Ga$_2$O$_3$ can act as basic O^{2-} scavenger and form negatively charged tetrahedrally coordinated species: Ga$_2$O$_3$ + O^{2-} $\rightarrow$ 2[GaO$_{4/2}$]$^-$, whereas Cs$_2$O releases basic O^{2-} to the melt: Cs$_2$O $\rightarrow$ 2Cs$^+$ +O^{2-}. This can be described as: Cs$_2$O + Ga$_2$O$_3$ $\rightarrow$ 2Cs$^+$ + 2[GaO$_{4/2}$]$^-$. Stoichiometric CsGaGe$_2$O$_6$ cannot provide much acidic species for capturing O^{2-} and stabilize Bi$^+$, this also explains why gallium excess sample contains relatively large concentration of NIR PL Bi$^+$ centers (Romanov et al., 2019).

Brief Summary

Regarding the improvement in Bi-doped NIR crystals, all the known crystals have been listed in Table 1, which are divided into two main categories of halogen and oxides compounds. These NIR Bi crystals can also be divided into two groups, although not shown here, as single crystal and polycrystal. As for the synthesis of single crystals, most researchers choose the Bridgman method because of its simple and mature process. To prepare polycrystals, the widely used method is the solid reaction method, and this can achieve industrialized mass production. Both NIR intensities should be stronger than that in glass systems, but Bi-doped NIR glasses may be better in optical transparency. In terms of choosing the host systems, however, one can note that nearly all the known NIR Bi crystals cannot escape this shackle that the host cations such as Ba^{2+}, Pb^{2+}, K$^+$, or Cs$^+$, which are generally large in size, can stabilize these luminescence centers. And this rule can be confirmed by the usually large ion radii of reported NIR Bi active centers such as Bi^{2+} (1.14 Å), Bi$^+$ (1.45 Å), and Bi^0 (1.60 Å) (Shannon, 1976).
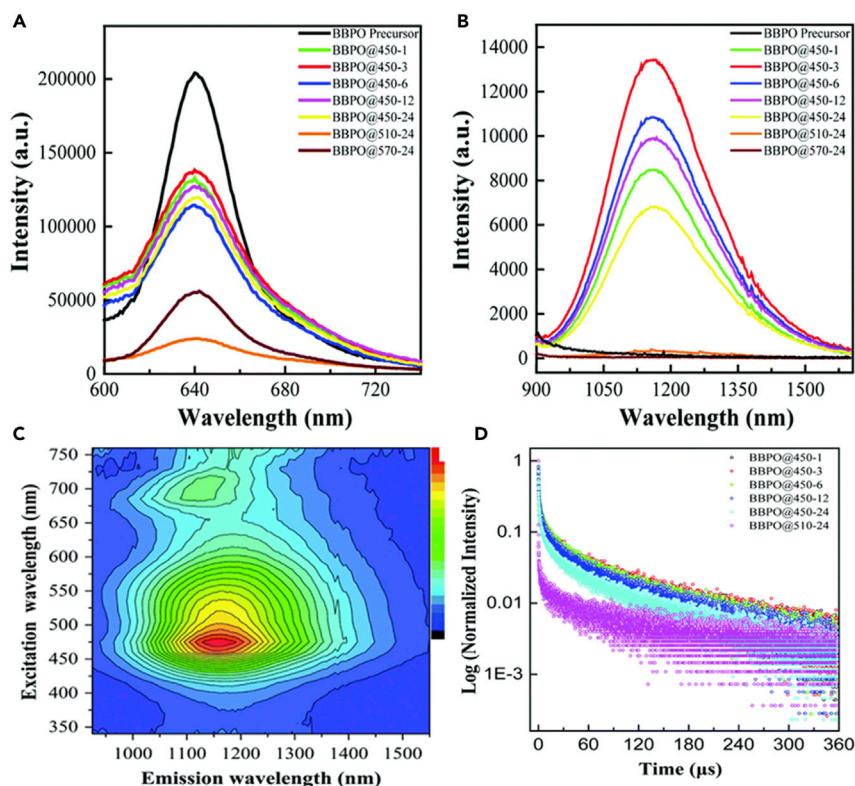
Figure 24. NIR Luminescent Properties of Bi:BBPO

(A) PL spectra of the precursor and reduced samples. Visible emission spectra excited at 407 nm.

(B) NIR emission spectra excited at 476 nm.

(C) Excitation-emission graph of the BBPO@450-3 sample.

(D) Decay curves for the reduced samples. Measurements were performed by monitoring the decay of the emission at 1,164 nm upon 476 nm excitation. Reproduced with permission (Liu et al., 2016). Copyright 2016, The Royal Society of Chemistry.

Unfortunately, due to the lack of systemic comparison of the coordination number information of these substituted lattice sites, one cannot precisely evaluate the Shannon ionic radii difference between the substituted cation and Bi^{3+} ions, and thus further targeted component design before synthesis may be impossible, but much labor has to be wasted in trial-and-error experiments. With the help of some software such as Findit and Diamond, we have perfected these information in the table for better comparison. From the table, one can clearly see that the emitters of NIR emission vary such as in Bi^{2+}, Bi^+, $[BiO_x]$, and Bi^0, and some researchers also think the NIR emissions in Bi-activated CsI and $CsPbI_3$ are attributed to Bi-induced defects such as color centers and polaronic defects, respectively (Su et al., 2011; Zhou et al., 2016). In all, most research work insist on the fact that Bi^+ accounts for NIR luminescence in Bi crystals. Due to the similarity of Bi^+ PL excitation and emission spectra in different crystals, one may irresponsibly conclude that the crystal effect has limited influence on the optical parameters. However, without crystal field, the $^3P_0$ ground state of Bi^+ can be nondegenerate, and the lowest excited states of $^3P_1$ (NIR range) and $^3P_2$ (visible range) are 3-fold and 5-fold without any splitting, respectively. Here, although Vtyurina et al. have realized the importance of crystal field on optical properties of NIR Bi^+ centers, one cannot get convincing conclusion regarding which crystal system, space group or point symmetry, is more suitable in producing NIR emission of Bi-doped crystals; further studies are required besides chlorides (Vtyurina et al., 2016). Obviously, one can note that higher coordination number with larger lattice site size should be better for NIR Bi centers.

Here, another point that should be focused on is that the valence of nearly each substituted cation is lower than 3+ (the most stable valence of Bi in the form of Bi_2O_3), except for Y^{3+} in Y_4GeO_8 (Xu et al., 2011) and P^{5+} and B^{3+} in $BaBPO_5$ (Liu et al., 2016). Here, reducing conditions (atmospheres or agents) are usually required during the synthesis process such as topotactic reduction of Bi-activated red-emitting crystals in $BaBPO_5$
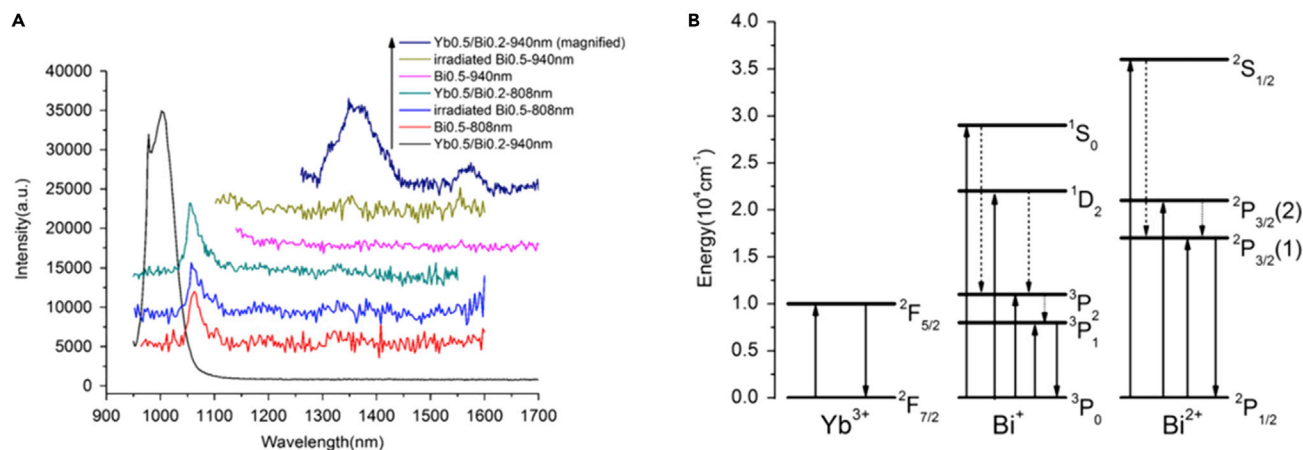
Figure 25. NIR Luminescent Properties of Bi:PbWO₄

(A) NIR emission spectra detected by 808-nm and 940-nm laser pumping.

(B) Energy level diagram of Yb^{3+}, Bi^+, and Bi^{2+}. Reproduced with permission (Xiong et al., 2012). Copyright 2012, Elsevier.

using Al powder. Usually, if the valence of cation to be substituted is lower than 3+, NIR luminescence of Bi centers may be stable. Thus, it is confusing in Y_4GeO_8 because they do not provide conclusion regarding any reduction conditions during synthesis and the valence of Y is 3 + here. As of today, it is a general consensus that tri- or higher-valence Bi ions are not the origin of NIR emission, as agreed with that in glass (Peng et al., 2011). However, the NIR emissions of Bi^{3+} have recently been confirmed by designing Bi^{3+} in $XAl_{12}O_{19}$ (Wei et al., 2020.). Finally, the decay times vary from several to several hundreds of microsecond (μs). Meanwhile, some interesting phenomena can be addressed here: we note that some single Bi ion-doped crystals will emit less or even nothing unless sensitized or stabilized by other co-dopants. For example, in Bi-doped $PbWO_4$, no NIR emission can be obtained. However, the authors found efficient NIR luminescence if co-doped with Yb^{3+} ions, in which energy transfer from Yb to Bi should explain this phenomenon (Xiong et al., 2012). Another way to enhance NIR emission has also been reported in Bi/Ta co-doped $Gd_{0.1}Y_{0.9}AlO_3$ single crystal, because the introduction of Ta^{5+} can effectively lead to the change of valence states from Bi^{3+} to Bi^+ based on the charge compensation mechanism (Zhang et al., 2018a, 2018b).
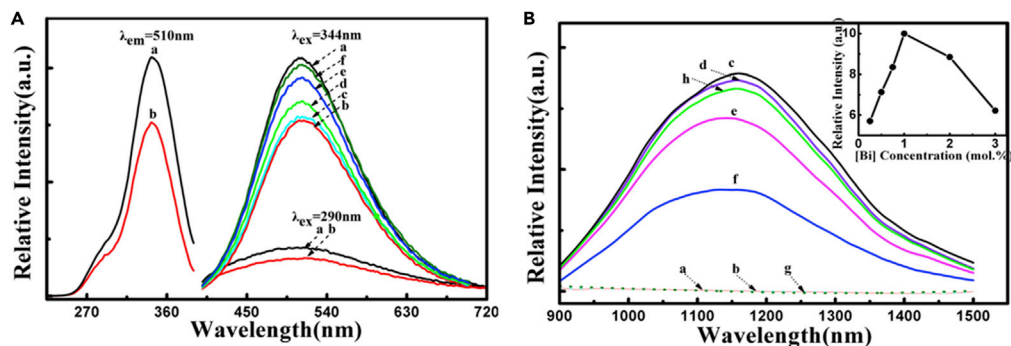

Figure 26. Luminescent Properties of Bi:Y₄GeO₈

(A) (Color online) Excitation (λ_{em} = 510 nm) and emission (λ_{ex} = 290, 344 nm) spectra of γ-ray unirradiated, irradiated, and heat-treated samples. (a) 1A, (b) 1R, (c) 1R100, (d) 1R200, (e) 1R300, (f) 1R350.

(B) NIR emission spectra of (a) 1A, (b) 0R (dotted line), (c) 1R, (d) 1R100, (e) 1R200, (f) 1R300, (g) 1R350, (h) 1RL excited by 808-nm laser diode (1RL was prepared by preserving sample 1R at room temperature in air for 2.5 months). The inset shows the relative NIR luminescence intensity as a function of x for γ-ray irradiated $(Y_{1-x}Bi_x)_4GeO_8$ (x = 0.0025, 0.005, 0.0075, 0.01, 0.02, 0.03) crystals excited by 808-nm laser diode. Reproduced with permission (Xu et al., 2011). Copyright 2011, The Electrochemical Society.
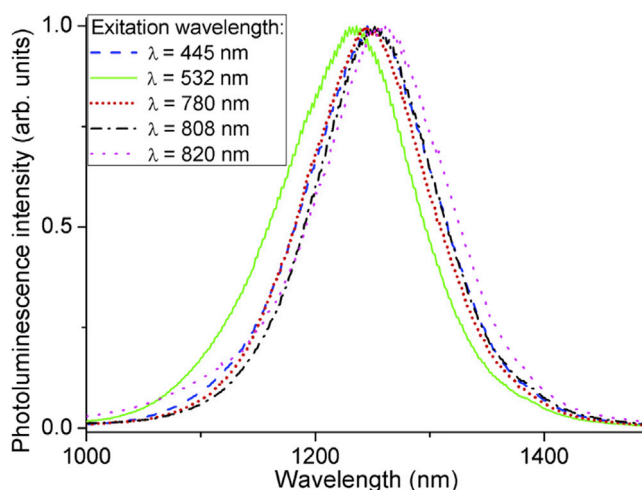
Figure 27. Photoluminescence Emission Spectra of Bi⁺-Doped CsGaGe₂O₆ (1:1.054CsGaGe₂O₆:Bi Specimen) under Different Excitation Wavelengths.
Reproduced with permission (Romanov et al., 2019). Copyright 2019, Elsevier.

CONCLUSIONS AND OUTLOOK

As a possible gain medium in fiber laser, Bi-doped NIR luminescent crystals have been developed in the past decades. In this review, all the known NIR Bi crystals have been collected and listed in Table 1. Although extensive studies have been performed on various chlorides and oxides, there are lots of spaces in exploiting NIR Bi crystals for practical applications, and the following challenges are remain to be addressed:

1) Gaining more insights into the structure information of the chosen hosts. In Table 1, we have tried our best to add the missed data; however, before this, few researches have provided detailed structure information of host such as crystal system, space group, or point symmetry. And the chemical environment data around the substituted sites in terms of coordination number and Shannon radii are always ignored. Hence, Rietveld refinement method should be urgently introduced to analyze the structure properties of lattice sites for Bi to substitute. Afterward, one need to further confirm these structure information with the help of some characterization techniques such as, but not limited to, EXAFS, XANES, and XPS. Only after we know where the Bi ions can be substituted for and what is the chemical environment around the sites, can we choose an NIR Bi crystal host rationally.

2) Detailed spectroscopic properties of doped Bi ions should be provided. Similar to structure information of host, most researches failed to provide the spectral data of doped Bi NIR centers. One can clearly note emissions centered at ~1,100 nm under the excitation of 400–940 nm lights, but the decay lifetimes were always missing; even these data can be a valid tool to confirm the nature of these NIR centers. Besides, the detailed charge-carrier dynamics in those crystals would also help investigate the nature of NIR luminescence. Thus, it is suggested to provide the time-resolved data.

3) Developing more ways to produce NIR emissions. In this review, two kinds of high-energy beam irradiation and energy transfer were found to induce NIR luminescence of Bi. First, as discussed in α-BaB₂O₄, PbWO₄, and Y₄GeO₈, only γ-ray irradiated samples can generate NIR luminescence of Bi in crystals. Moreover, it has been confirmed that these NIR emissions can be bleached at higher temperature. Such a method should be focused on, but not limited to, if one aims to selectively produce or erase the NIR signals of Bi in crystals. Second, the efficient energy transfer from Yb³⁺ to Bi⁺ active centers made PbWO₄ another NIR Bi crystal. So, if one can find more energy transfer routes between low-valence Bi and other ions or even hosts, it would be highly desirable in designing novel NIR Bi crystals.

4) Developing more ways to enhance or tune the NIR emission. Although there has been strategy to increase the NIR luminescence intensity by codoping, for example, the codoping with Ta⁵⁺ ions could enhance the NIR emission of Bi⁺ at least two times in Bi: Gd₀.₁Y₀.₉AlO₃, other researches

that can be referred to are limited. Hence, it is suggested that researches about how to optimize NIR luminescence intensity should be systematically carried on. In addition, as Bi-doped NIR crystals may be used as more efficient gain media or source materials in modern communication systems, it is expected that these emissions could be highly tuned. Developing ways to tune its NIR emission should be worth doing, and doping NIR Bi centers into multiple lattice sites may be a choice.

5) Considering the nature of NIR emitters in crystals, it is widely accepted that low-valence Bi ion models such as Bi^{2+}, Bi^+, and Bi^0 can be considered, of which Bi^+ is the most popular recognized. However, some researches also attributed the NIR emission of Bi to other centers such as color center or polaronic defect. Personally, future work is suggested to provide undisputable experimental data if they insist on proposing another kind of NIR Bi model.

6) To further explore practical applications of NIR Bi crystals. Fallaciously, no practical application display has been provided in the past published work. However, Bi-doped NIR crystals should at least be used as a high-quality optical amplifier gain media compared with glass in optical fiber telecommunication. Moreover, it would be amazing if one can exploit a Bi-doped NIR crystal with rationally tunable NIR emission. In all, more practical applications are needed to be exploited.

7) To discuss the influence of single crystal or polycrystalline materials on corresponding Bi NIR emissions. From the published work, one can easily note that both Bi-doped single crystal and polycrystalline materials could be proper hosts to stabilize NIR Bi active center. However, the two categories are quite different in terms of various aspects such as grain size, grain boundary, and local disorder. So if one can carefully compare the emission efficiency of same Bi NIR center in both systems, we believe this work would be highly worth.

In all, a number of Bi-activated NIR luminescent crystals are still in the research stage. Comprehensive crystal structure information of host materials and emitter will be highly desirable, and it is believed that more applications of Bi NIR crystals will be confirmed in the near future.

Search Strategy and Selection Criteria

Data for this review were identified by searches of Web of Science, PubMed, Google Scholar, and references from relevant articles using the search terms "bismuth (Bi)," "near infrared (NIR)," and "crystal." Only articles published in English were included.

AUTHOR CONTRIBUTIONS

Conceptualization: P.X., Y.L., and M.P., Writing – Original Draft: P.X. and Y.L., Visualization: M.P., Supervision: M.P.

REFERENCES

Blasse, G., Meijerink, A., Nomes, M., and Zuidema, J. (1994). Unusual bismuth luminescence in strontium tetraborate. J. Phys. Chem. Sol. 55, 171–174.

Cao, J., Li, L., Wang, L., Li, X., Zhang, Z., Xu, S., and Peng, M. (2018a). Creating and stabilizing Bi NIR-emitting centers in low Bi content materials by topo-chemical reduction and tailoring of the local glass structure. J. Mater. Chem. C 6, 5384–5390.

Cao, J., Wondraczek, L., Wang, Y., Wang, L., Li, J., Xu, S., and Peng, M. (2018b). Ultrabroadband near-infrared photoemission from Bismuth centers in nitridated oxide glasses and optical fiber. ACS Photonics 5, 4393–4401.

Cao, J., Xu, S., Zhang, Q., Yang, Z., and Peng, M. (2018c). Ultrabroad photoemission from an amorphous solid by topochemical reduction. Adv. Opt. Mater. 6, 1801059.

Cao, J., Peng, J., Wang, L., Luo, H., Wang, X., Xiong, P., Wang, Y., and Peng, M. (2019). Broadband NIR emission from multiple Bi centers in nitridated borogermanate glasses via tailoring local glass structure. J. Mater. Chem. C 7, 2076–2084.

Chen, N., Zhang, P., Yin, H., Zhu, S., Li, Z., and Chen, Z. (2018a). Near infrared broadband emission of a new bismuth-doped $Gd_{0.1}Y_{0.9}AlO_3$ crystal. Infrared Phys. Technol. 94, 214–218.

Dianov, E.M., Dvoyrin, V.V., Mashinsky, V.M., Umnikov, A.A., Yashkov, M.V., and Gur'yanov, A.N. (2005). CW bismuth fibre laser. Quan. Electron. 35, 1083–1084.

Dvoyrin V., Mashinsky, V., Dianov, E., Umnikov, A., Yashkov, M., and Guryanov, A. (2005). Absorption, fluorescence and optical amplification in MCVD bismuth-doped silica glass optical fibres. Paper presented at: 2005 31st

European Conference on Optical Communication, ECOC 2005 (IET).

Fermann, M.E., and Hartl, I. (2013). Ultrafast fibre lasers. Nat. Photon. 7, 868–874.

Firstov, S.V., Zhao, M., Su, L., Yang, Q., Iskhakova, L.D., Firstova, E.G., Alyshev, S.V., Riumkin, K.E., and Dianov, E.M. (2016). Optical properties of bismuth-doped KCl and SrF_2 crystals. Laser Phys. 26, 096201.

Fockelet, M., Lohse, F., Spaetht, J.M., and Bartram, R.H. (1989). Identification and optical properties of axial lead centres in alkaline-earth fluorides. Condens Matter 1, 13–26.

Fujimoto, Y., and Nakatsuka, M. (2001). Infrared luminescence from bismuth-doped silica glass. Jpn. J. Appl. Phys. 40, L279–L281.

Fujimoto, Y., and Nakatsuka, M. (2003). Optical amplification in bismuth-doped silica glass. Appl. Phys. Lett. 82, 3325–3326.

Gelleilmann, W., and Luty, F. (1981). Optical properties and stable broadly tunable CW laser opteration of new FA-type centers in Tl^+ doped alkalihalides. Opt. Commun. 39, 391–395.

Krasnikov, A., Mihokova, E., Nikl, M., Zazubovich, S., and Zhydachevskyy, Y. (2020). Luminescence spectroscopy and origin of luminescence centers in Bi-doped materials. Crystals 10, 208.

Li, C., Song, Z., Qiu, J., Yang, Z., Yu, X., Zhou, D., Yin, Z., Wang, R., Xu, Y., and Cao, Y. (2012). Broadband yellow–white and near infrared luminescence from Bi-doped $Ba_{10}(PO_4)_6Cl_2$ prepared in reductive atmosphere. J. Lumin. 132, 1807–1811.

Li, C., Li, Y., Wang, X., Wang, Q., Song, Z., Qiu, J., Zhao, Z., Yang, Z., Yin, Z., and Zhou, D. (2013). Study on the effect of apatite structure on spectroscopic properties of bismuth activated alkaline earth metal chlorophosphate $[M_5(PO_4)_3Cl; M = Ca, Sr$ and Ba]. Mater. Chem. Phys. 139, 220–224.

Liu, B.-M., Yong, Z.-J., Zhou, Y., Zhou, D.-D., Zheng, L.-R., Li, L.-N., Yu, H.-M., and Sun, H.-T. (2016). Creation of near-infrared luminescent phosphors enabled by topotactic reduction of bismuth-activated red-emitting crystals. J. Mater. Chem. C 4, 9489–9498.

Meng, X.G., Qiu, J.R., Peng, M.Y., Chen, D.P., Zhao, Q.Z., Jiang, X.W., and Zhu, C.S. (2005). Near infrared broadband emission of bismuth-doped aluminophosphate glass. Opt. Express 13, 1628–1634.

Murata, K., Fujimoto, Y., Kanabe, T., Fujita, H., and Nakatsuka, M. (1999). Bi-doped SiO_2 as a new laser material for an intense laser. Fusion Eng. Des. 44, 437–439.

Okhrimchuk, A.G., II., Butvina, L.N., Dianov, E.M., Lichkova, N.V., Zagorodnev, V.N., and Boldyrev, K.N. (2008). Near-infrared luminescence of $RbPb_2Cl_5$:Bi crystals. Opt. Lett. 33, 2182–2184.

Peng, M., and Wondraczek, L. (2009). Bismuth-doped oxide glasses as potential solar spectral converters and concentrators. J. Mater. Chem. 19, 627–630.

Peng, M.Y., Qiu, J.R., Chen, D.P., Meng, X.G., Yang, I.Y., Jiang, X.W., and Zhu, C.S. (2004). Bismuth- and aluminum-codoped germanium oxide glasses for super-broadband optical amplification. Opt. Lett. 29, 1998–2000.

Peng, M., Qiu, J., Chen, D., Meng, X., and Zhu, C. (2005). Superbroadband 1310 nm emission from bismuth and tantalum codoped germanium oxide glasses. Opt. Lett. 30, 2433–2435.

Peng, M., Chen, D., Qiu, J., Jiang, X., and Zhu, C. (2007). Bismuth-doped zinc aluminosilicate glasses and glass-ceramics with ultra-broadband infrared luminescence. Opt. Mater. 29, 556–561.

Peng, M., Zollfrank, C., and Wondraczek, L. (2009). Origin of broad NIR photoluminescence in bismuthate glass and Bi-doped glasses at room temperature. J. Phys. Condens Matter 21, 285106.

Peng, M., Sprenger, B., Schmidt, M.A., Schwefel, H.G.L., and Wondraczek, L. (2010). Broadband NIR photoluminescence from Bi-doped $Ba_2P_2O_7$ crystals: insights into the nature of NIR-emitting bismuth centers. Opt. Express 18, 12852–12863.

Peng, M., Dong, G., Wondraczek, L., Zhang, L., Zhang, N., and Qiu, J. (2011). Discussion on the origin of NIR emission from Bi-doped materials. J. Non-crystalline Sol. 357, 2241–2245.

Plotnichenko, V.G., Sokolov, V.O., Philippovskiy, D.V., Golovanov, V.F., Polyakova, G.V., Lisitsky, I.S., and Dianov, E.M. (2013a). Infrared luminescence in bismuth-doped AgCl crystals. Opt. Lett. 38, 2965–2968.

Plotnichenko, V.G., Sokolov, V.O., Philippovskiy, D.V., Lisitsky, I.S., Kouznetsov, M.S., Zaramenskikh, K.S., and Dianov, E.M. (2013b). Near-infrared luminescence in TlCl:Bi crystal. Opt. Lett. 38, 362–364.

Romanov, A.N., Fattakhova, Z.T., Veber, A.A., Usovich, O.V., Haula, E.V., Korchak, V.N., Tsvetkov, V.B., Trusov, L.A., Kazin, P.E., and Sulimov, V.B. (2012). On the origin of near-IR luminescence in Bi-doped materials (II). Subvalent monocation Bi^+ and cluster Bi_5^{3+} luminescence in $AlCl_3/ZnCl_2/BiCl_3$ chloride glass. Opt. Express 20, 7212–7220.

Romanov, A.N., Veber, A.A., Fattakhova, Z.T., Usovich, O.V., Haula, E.V., Trusov, L.A., Kazin, P.E., Korchak, V.N., Tsvetkov, V.B., and Sulimov, V.B. (2013). Subvalent bismuth monocation $Bi+$ photoluminescence in ternary halide crystals $KAlCl_4$ and $KMgCl_3$. J. Lumin. 134, 180–183.

Romanov, A.N., Veber, A.A., Fattakhova, Z.T., Vtyurina, D.N., Kouznetsov, M.S., Zaramenskikh, K.S., Lisitsky, I.S., Korchak, V.N., Tsvetkov, V.B., and Sulimov, V.B. (2014). Spectral properties and NIR photoluminescence of Bi^+ impurity in $CsCdCl_3$ ternary chloride. J. Lumin. 149, 292–296.

Romanov, A.N., Veber, A.A., Vtyurina, D.N., Fattakhova, Z.T., Haula, E.V., Shashkin, D.P., Sulimov, V.B., Tsvetkov, V.B., and Korchak, V.N. (2015a). Near infrared photoluminescence of the univalent bismuth impurity center in leucite and pollucite crystal hosts. J. Mater. Chem. C 3, 3592–3598.

Romanov, A.N., Veber, A.A., Vtyurina, D.N., Kouznetsov, M.S., Zaramenskikh, K.S., Lisitsky, I.S., Fattakhova, Z.T., Haula, E.V., Loiko, P.A., Yumashev, K.V., et al. (2015b). NIR photoluminescence of bismuth-doped $CsCdBr_3$ – the first ternary bromide phase with a univalent bismuth impurity center. J. Lumin. 167, 371–375.

Romanov, A.N., Vtyurina, D.N., Haula, E.V., Shashkin, D.P., Pimkin, N.A., Kuznetsov, M.S., Lisitsky, I.S., and Korchak, V.N. (2016). IR photoluminescence of Bi^+ impurity centers in the RbY_2Cl_7 ternary chloride. Russ. J. Phys. Chem. B 10, 735–739.

Romanov, A.N., Vtyurina, D.N., Haula, E.V., Shashkin, D.P., Pimkin, N.A., Kuznetsov, M.S., Lisitsky, I.S., and Korchak, V.N. (2017). Broadband infrared photoluminescence of $TlCdI_3$ iodide doped with bismuth. Russ. J. Phys. Chem. B 11, 83–86.

Romanov, A.N., Haula, E.V., Boldyrev, K.N., Shashkin, D.P., and KorchaK, V.N. (2019). Broadband Near-IR photoluminescence of bismuth-doped pollucite-related phase $CsGaGe_2O_6$. J. Lumin. 26, 116741.

Ruan, J., Su, L., Qiu, J., Chen, D., and Xu, J. (2009). Bi-doped BaF_2 crystal for broadband near-infrared light source. Opt. Express 17, 5163–5169.

Shannon, R. (1976). Revised effective ionic radii and systematic studies of interatomic distances in halides and chalcogenides. Acta Crystallogr. A 32, 751–767.

Snitzer, E. (1961). Optical maser action of Nd3+ in a barium crown glass. Phys. Rev. Lett. 7, 444.

Su, L., Yu, J., Zhou, P., Li, H., Zheng, L., Yang, Y., Wu, F., Xia, H., and Xu, J. (2009a). Broadband near-infrared luminescence in γ-irradiated Bi-doped α-BaB_2O_4 single crystals. Opt. Lett. 34, 2504–2506.

Su, L., Zhao, P., Yu, J., Li, H., Zheng, L., Wu, F., Yang, Y., Yang, Q., and Xu, J. (2009b). Spectroscopic properties and near-infrared broadband luminescence of Bi-doped SrB_4O_7 glasses and crystalline materials. Opt. Express 17, 13554–13560.

Su, L., Zhao, H., Li, H., Zheng, L., Ren, G., Xu, J., Ryba-Romanowski, W., Lisiecki, R., and Solarz, P. (2011). Near-infrared ultrabroadband luminescence spectra properties of subvalent bismuth in CsI halide crystals. Opt. Lett. 36, 4551–4553.

Sun, H.-T., Zhou, J., and Qiu, J. (2014). Recent advances in bismuth activated photonic materials. Prog. Mater. Sci. 64, 1–72.

Udem, T., Holzwarth, R., and Hänsch, T.W. (2002). Optical frequency metrology. Nature 416, 233–237.

Veber, A.A., III., Romanov, A.N., Usovich, O.V., Fattakhova, Z.T., Haula, E.V., Korchak, V.N., Trusov, L.A., Kazin, P.E., Sulimov, V.B., and Tsvetkov, V.B. (2012). Luminescent properties of Bi-doped polycrystalline $KAlCl_4$. Appl. Phys. B 108, 733–736.

Vtyurina, D.N., Romanov, A.N., Veber, A.A., Fattakhova, Z.T., Antonov, A.A., Tsvetkov, V.B., and Korchak, V.N. (2016). The spectral properties and the NIR photoluminescence of univalent bismuth Bi^+ in $RbAlCl_4$, $CsAlCl_4$, $RbMgCl_3$, $CsMgCl_3$, $KCdCl_3$ and $RbCdCl_3$ crystal phases. Russ. J. Phys. Chem. B 10, 388–393.

Wang, L., Long, N.J., Li, L., Lu, Y., Li, M., Cao, J., Zhang, Y., Zhang, Q., Xu, S., Yang, Z., et al. (2018a). Multi-functional bismuth-doped bioglasses: combining bioactivity and photothermal response for bone tumor treatment and tissue repair. Light Sci. Appl. 7, 1.

Wang, X., Boutinaud, P., Li, L., Cao, J., Xiong, P., Li, X., Luo, H., and Peng, M. (2018b). Novel persistent and tribo-luminescence from bismuth ion pairs doped strontium gallate. J. Mater. Chem. C 6, 10367–10375.

Wang, X., Xu, S., Yang, Z., and Peng, M. (2019b). Ultra-broadband red to NIR photoemission from multiple bismuth centers in $Sr_2B_5O_9Cl$:Bi crystal. Opt. Lett. 44, 4821–4824.

Wei, Y., Gao, Z., Yun, X., Yang, H., Liu, Y., and Li, G. (2020). Abnormal Bi^{3+}-activated NIR emission in highly symmetric $XAl_{12}O_{19}$ (X = Ba, Sr, Ca) by selective sites occupation. Chem. Mater. https://doi.org/10.1021/acs.chemmater.0c02814.

Wolfert, A., and Blasse, G. (1984). Luminescence of s^2 ions in $CsCdBr_3$ and $CsMgCl_3$. J. Solid State Chem. 55, 344–352.

Xia, H.-P., and Wang, X.-J. (2006). Near infrared broadband emission from Bi5+-doped Al2O3–GeO2–X (X=Na2O,BaO,Y2O3) glasses. Appl. Phys. Lett. 89, 051917.

Xiong, W., Yuan, H., Su, L., Chen, L., Zhou, Y., Luo, C., and Yang, Y. (2012). Growth and near-infrared luminescence properties of Yb–Bi co-doped $PbWO_4$ crystal. J. Cryst. Growth 358, 29–32.

Xiong, P., Zheng, C., Peng, M., Zhou, Z., Xu, F., Qin, K., Hong, Y., and Ma, Z. (2020). Self-activated persistent luminescence from $Ba_2Zr_2Si_3O_{12}$ for information storage. J. Am. Cera Soc. 124, 063101.

Xu, J., Zhao, H., Su, L., Yu, J., Zhou, P., Tang, H., Zheng, L., and Li, H. (2010). Study on the effect of heat-annealing and irradiation on spectroscopic properties of Bi:α-BaB_2O_4 single crystal. Opt. Express 18, 3385–3391.

Xu, B., Tan, D., Guan, M., Teng, Y., Zhou, J., Qiu, J., and Hong, Z. (2011). Broadband near-infrared luminescence from γ-ray irradiated bismuth-doped Y_4GeO_8 crystals. J. Electrochem. Soc. 158, G203–G206.

Zhang, P., Chen, N., Wang, R., Huang, X., Zhu, S., Li, Z., Yin, H., and Chen, Z. (2018a). Charge compensation effects of Yb^{3+} on the Bi^+: near-infrared emission in PbF_2 crystal. Opt. Lett. 43, 2372–2375.

Zhang, P., Chen, N., Zhu, S., Li, Z., Chen, Z., Zheng, Y., and Yu, J. (2018c). Efficient enhancement of bismuth near infrared luminescence by the co-doping of tantalum in GYAP crystal. Opt. Express 26, 23207–23214.

Zheng, J., Peng, M., Kang, F., Cao, R., Ma, Z., Dong, G., Qiu, J., and Xu, S. (2012). Broadband NIR luminescence from a new bismuth doped $Ba_2B_5O_9Cl$ crystal: evidence for the Bi^0 model. Opt. Express 20, 22569–22578.

Zheng, J., Tan, L., Wang, L., Peng, M., and Xu, S. (2016). Superbroad visible to NIR photoluminescence from Bi^+ evidenced in $Ba_2B_5O_9Cl$: Bi crystal. Opt. Express 24, 2830–2835.

Zheng, C., Xiong, P., Peng, M., and Liu, H. (2020). Discovery of novel rare-earth free narrow-band blue-emitting phosphor $Y_3Al_2Ga_3O_{12}$: Bi^{3+} with strong NUV excitation for LCD LED backlights. J. Mater. Chem. C 7, 3730–3734.

Zhou, Y., Zhou, D.-D., Liu, B.M., Li, L.N., Yong, Z.J., Xing, H., Fang, Y.Z., Hou, J.Z., and Sun, H.T. (2016). Ultrabroad near-infrared photoluminescence from bismuth doped $CsPbI_3$: polaronic defects vs. bismuth active centers. J. Mater. Chem. C 4, 2295–2301.

Zhou, G., Jiang, X., Zhao, J., Molokeev, M., Lin, Z., Liu, Q., and Xia, Z. (2018). Two dimensional layered perovskite $ALaTa_2O_7$:Bi^{3+} (A = K and Na) phosphors with versatile structures and tunable photoluminescence. ACS Appl. Mater. Interfaces 10, 24648–24655.

Zhou, Z., Xiong, P., Liu, H., and Peng, M. (2020). Ultraviolet-a persistent luminescence of a Bi^{3+}-activated $LiScGeO_4$ material. Inorg. Chem. 59, 12920–12927.